This project has received funding from the European Union's Seventh Programme for research, technological development and demonstration under grant agreement No [308417]".

New Directions in Seismic Hazard Assessment through Focused Earth Observation in the Marmara Supersite

Grant Agreement Number: 308417
co-funded by the European Commission within the Seventh Framework Programme
THEME [ENV.2012.6.4-2]
[Long-term monitoring experiment in geologically active regions of Europe prone to natural hazards: the Supersite concept]

D6.3
Report on numerical modelling of ground motion and local site effects

Project Start Date	1 November 2012
Project Duration	42 months
Project Coordinator /Organization	Nurcan Meral Özel / KOERI
Work Package Number	WP6
Deliverable Name/ Number	Report on numerical modeling of ground motion and local site effects
Due Date Of Deliverable	Month 30
Actual Submission Date	29/04/2016
Organization/Author (s)	INERIS/S. COCCIA, P. BIGARRE

Dissemination Level		
PU	Public	
PP	Restricted to other programme participants (including the Commission)	
RE	Restricted to a group specified by the consortium (including the Commission)	
CO	Confidential, only for members of the consortium (including the Commission)	

TABLE OF CONTENTS

1 INTRODUCTION

Earthquake-triggered landslides have an increasing disastrous impact in seismic regions due to the fast growing urbanization and infrastructures. Just considering disasters from the last fifteen years, among which the 1999 Chi-Chi earthquake, the 2008 Wenchuan earthquake, and the 2011 Tohoku earthquake, these events generated tens of thousands of coseismic landslides. Those resulted in amazing death toll and considerable damages, affecting the regional landscape including its hydrological main features.

Despite a strong impetus in research during past decades, knowledge on those geohazards is still fragmentary, while databases of high quality observational data are lacking. These phenomena call for further collaborative researches aiming eventually to enhance preparedness and crisis management.

As one of the three SUPERSITE concept FP7 projects dealing with long term high level monitoring of major natural hazards at the European level, the MARsite project gathers research groups in a comprehensive monitoring activity developed in the Sea of Marmara Region, one of the most densely populated parts of Europe and rated at high seismic risk level since the 1999 Izmit and Duzce devastating earthquakes. These earthquakes caused extensive landslides while tsunami effects were observed during the post-event surveys in several places along the coasts of the Izmit bay.

1.1 Overview of MARsite WP6

The 6th Work Package (Earthquake-induced landslide hazard in Marmara) of MARsite project gathers 9 research groups groups (INERIS, IU, ITU, TUBITAK, INGV, CNR, University of Pavia, IFSTTAR - University of “La Sapienza”) to study earthquake-induced landslides focusing on two sub-regional areas of high interest. First, the *Cekmece-Avcilar peninsula*, located westwards of Istanbul, is a highly urbanized concentrated landslide prone area, showing high susceptibility to both rainfalls while affected by very significant seismic site effects. Second, *the off-shore entrance of the Izmit Gulf*, close to the termination of the surface rupture of the 1999 earthquake, that shows an important slump mass facing the Istanbul coastline.

The aim of this work package is to improve the preparedness of those seismically induced landslide geohazards, through the using and the improvement of monitoring and observing systems in hydrogeological and seismically well-constrained areas within the supersite.

The on-shore area was the object of analyses for tasks 1b (investigations of local instability areas and developing of advanced susceptibility mapping for on-shore landslides) and 2b (ground motion data, local seismic site effects and dynamic numerical modelling for on-shore landslides). In the on-shore area one representative pilot site of unstable slope (called Buyukcekmece landslide) was selected to set up a temporary multi-parameter ground monitoring as well as the in-depth slope stability analysis based on the stress-strain dynamic numerical modelling approach.

The results of the task 1b were showed in the deliverables D6.1.

The deliverable D6.3 summarizes the multidisciplinary scientific contributions and results obtained for the task 2b, that is focused on ground motion data and local seismic site effects at Buyukcekmece landslide.

The work subdivision for this task was the following:

- ✓ INERIS installed at Buyukcekmece landslide a local multi-paramter observational system, included a seismic network necessary to fill the gaps of available seismological catalogues to catch any microseismological activity;
- ✓ IU carried out geophysical measurements to investigate physical characteristics of the Buyukcekmece landslide;

- ✓ IFSTTAR-La Sapienza analyzed the local seismic response of the Buyukcekmece landslide before reconstructing a detailed engineering-geological model and then through a 2D numerical simulation in viscoelastic condition.

1.2 Deliverable approach

This deliverable is outlined as follows:

- Chapter 2: a prototype observational system, installed by INERIS, at Buyukcekmece landslide and the first time series collected are presented. These time series are directly accessible via an infrastructure of web-monitoring called "e-cenaris".
- Chapter 3: local site effects of Buyukcekmece landslide are showed. They are obtained through geophysical measurements and also computing the spectral ratios of earthquakes recorded by the local INERIS network.
- Chapter 4: the geophysical measurements and the geological field surveys in the landslide area were combined to obtain an engineering-geological model. This model was the starting point to analyze the local seismic response of Buyukcekmece landslide.
- Chapter 5: an overview of the results and gains thanks to the project is proposed, along with the potential future objectives to achieve. In addition, a list of the main publications is presented.

2 Local INERIS multi-parameter observational system

A prototype observational system was installed by INERIS, in collaboration with the IU, TUBITAK at the Büyükçekmece landslide on July 2014 (see Figure 1).

The Buyukcekmece landslide occurs in the form of two loops, the left and right loops are divided with a ridge. The right part constitutes the investigation site. It has about 1000 m width and 3000 m length. The slope on the landslide partly rises to 24%; the average is approximately 10%. This landslide has a continuous activity with low velocity, and it is classified as composite mechanism. It includes rototranslational parts, several secondary scarps, several landslide terraces (these last ones are characterized by an evident counter slope and some of them are responsible for the presence of water pools), evidences of two earth flows; the first one located along the right side of the landslide mass and the second one at its toe (these earth flows are clearly visible in the field due to the presence of detachment and transportation zones). Several evidences of damage to roads, buildings, walls, and infrastructures were also collected and considered for mapping the landslide mass.

Figure 1: Partial overview of the Buyukcekmece landslide (Istanbul, Turkey) from the roof terrace of the shopping center.

The temporary monitoring network is a multi-parameter type and consists in a seismic system, a geotechnical system and a GPS-RTK system (see Figure 2). This last one is based on the state of the art technologies of differential GPS, this station is designed for periodic 3D displacement measurements with a precision up to a couple of centimetres. Its rugged, wireless and low power consumption conception allows it to be easily deployed on the field in most situations. Because of its stability, it transmits measurement corrections to GPS measurement devices on the field, offering much better precision in the displacements. It is necessary that the radio antenna of each GPS station has a reasonable line-of-sight to the reference station and a distance less than 1 km.

Figure 2: Positions of the different sensors of the observational monitoring system (yellow line is the landslide contour).

GPS-RTK system is composed by:

- 1 reference GPS station, located in a steady renowned area, on the upper roof of a "Shopping center (SC) located upslope in a stable area (see Figure 2 for location).
- 2 measurement stations, installed in the landslide area: so-called "Farm" (FM) and "House" (HS) (see Figure 2 for location).

Seismic system consists in:

- two 3D seismic probes (installed at the bottom, -45m, and on the surface of a 70 meters deep borehole close to the farm station) called "Surf" and "Down" (or "SU" or "FO" by IFSTTAR-La Sapienza) to measure seismic ground motion (sensor type 2Hz GEOSPACE, bandwidth ±3dB, inherent sensibility 2 V/in/s) sampling at 1kHz with a threshold at 1.10^{-3}mm/s.

Geotechnical system consists in:

- 2 piezometers (vibrating wire technology) installed at the FM station measuring pore pressure at different depth (-36m and -51m) in the MARsite borehole with a measuring range 0-2 bar.
- 1 moisture sensor, installed at the FM station horizontally and about 30 cm deep.
- 1 rainfall meter and a temperature sensor at the HS station.

The instrumented borehole was drilled and equipped as part of a large scale geological and geotechnical survey of the area driven by the Istanbul Metropolitan Municipality and TUBITAK.

Digital raw data are concentrated to a SYTGEM-vlp acquisition unit which was also installed at the FM station. Data are transmitted in near to real-time using high speed cellular mobile network to an infrastructure featuring seamless data base management of raw data, processing and sharing both data and results of the monitoring through a dedicated web-monitoring secured page playing the role of a monitoring desk (e-cenaris).

All technical information and specifications about this monitoring system are synthetized into the deliverable D 9.2 (Prototype landslide early warning monitoring system for the Marmara region). This system has been calibrated and started to collect time series from October 20, 2014.

This monitoring aims first to collect time series on a large and slow landslide on the geological setting of the Avcilar peninsula for a better understanding of the landslide mechanism versus time, underground pore pressure and seismic ground motion.

Second, it is aimed to assess the technological integration of the system for both real-time warning (development of large displacements induced by a combination of precipitations and seismic ground motion) towards potential end-users in both situations: response of the mass during a major event, and response assessment after a major event for better decision making. Time series obtained in the near future will contribute to the development of procedures aiming at the detection and definition of a seismic landslide warning system.

2.1 First time-series

From October 2014 to December 2015 81 earthquakes were recorded with a maximum local magnitude of 6,1 and a minimum local magnitude of 1,7 and an epicentral distance ranging from 15 km to 676 km (Figure 3). The information about local magnitude comes from the KOERI website (http://www.koeri.boun.edu.tr/sismo/2/latest-earthquakes/list-of-latest-events/).

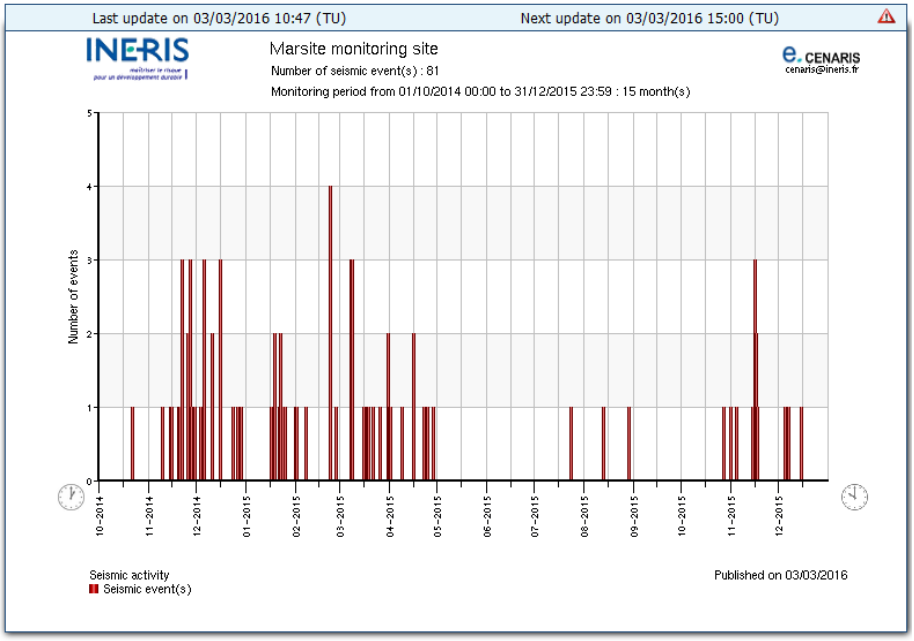

Figure 3: Seismic activity from October 2015 to December 2015.

As we can see in the figure 3 we had two gaps for the recorded seismic activity due to a technical problem with the acquisition unit. This first problem was solved thanks to an INERIS field visit and the second thanks to the help of the IU partners. The deep station is out of order since the summer 2015; its breakdown is due to a cut of the cable. We do not know the causes of this cut, one hypothesis is that it is due to the landsliding mass. Anyway, the maximum number of recorded events per day was 4 for both stations.

In addition, in the western part of Istanbul metropolitan area (Figure 4) there is another local seismic network composed of 8 seismic stations and operated by TUBITAK. The stations were deployed between Küçükçekmece and Büyükçekmece lakes in 2009 and two of them are still in the field, one of these is a reference station (TEPT station), installed on metamorphic rock outside the landslide area. The instruments are equipped with Lennartz 1Hz sensors and RefTek 130 dataloggers.

In the reference site approach, a reference station is set up on unweathered and horizontal bedrock. If this station is close to the station monitoring the study site, motions recorded by both of them for the same event likely contain similar source and path effects, so the comparison provides an estimate of site response effects. Methods for estimating

site response, generally, compare either response spectral ordinates or Fourier amplitude spectra.

The earthquakes recorded by the TEPT station, after correction for the instrument response, were compared with the records of the INERIS local network in term of peak ground velocity (PGV) and peak ground acceleration (PGA) for all the components at the same time (see Figure 5).

Then, to obtain an estimation of the amplification factor the PGA values of the INERIS deep and surface probes were compared with them of the reference station on rock (TEPT station). The distance between TEPT station and INERIS station is about 5 km.

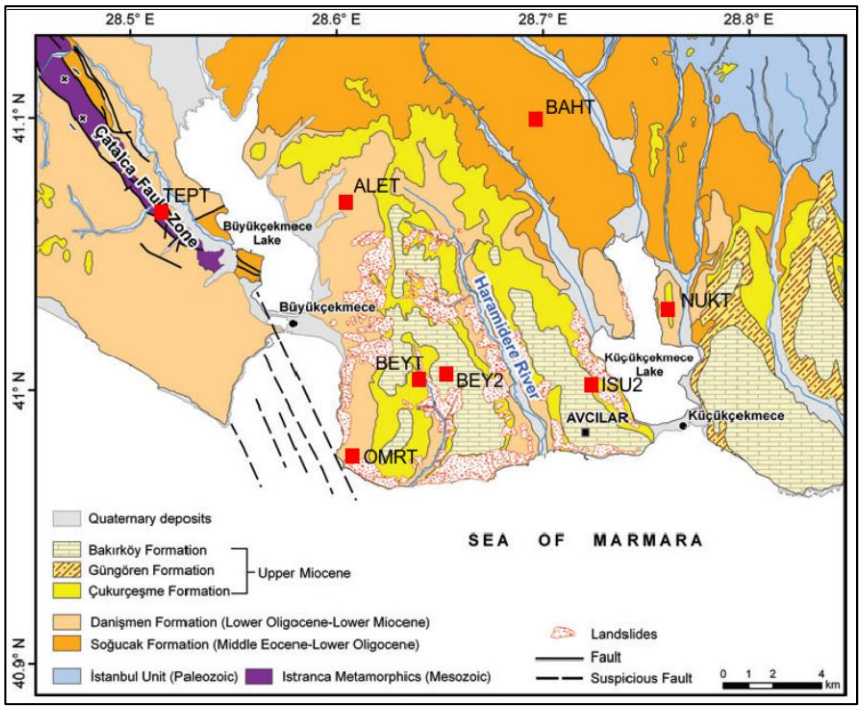

Figure 4: Geologic map of the study area and station locations (red squares) of the TUBITAK local seismic network.

For all local magnitude range the ratio between INERIS deep station and TEPT station is ≤ 0.2, the ratio between INERIS surface station and TEPT station is comprised between 0.05 and 0.6 (see

Figure **6**). According to these results there is no amplification of INERIS stations respect to the reference station (TEPT station), but surface station has PGA values major than deep station, so there is a local amplification along the vertical profile due to the depth. It is worth to notice that the deep station is locate above the probable sliding surface, so the vertical stratigraphic profile is the same for both stations. The absence of other stations in different points of the landslide area does not permit to study any kind of amplification due to the landslide mass.

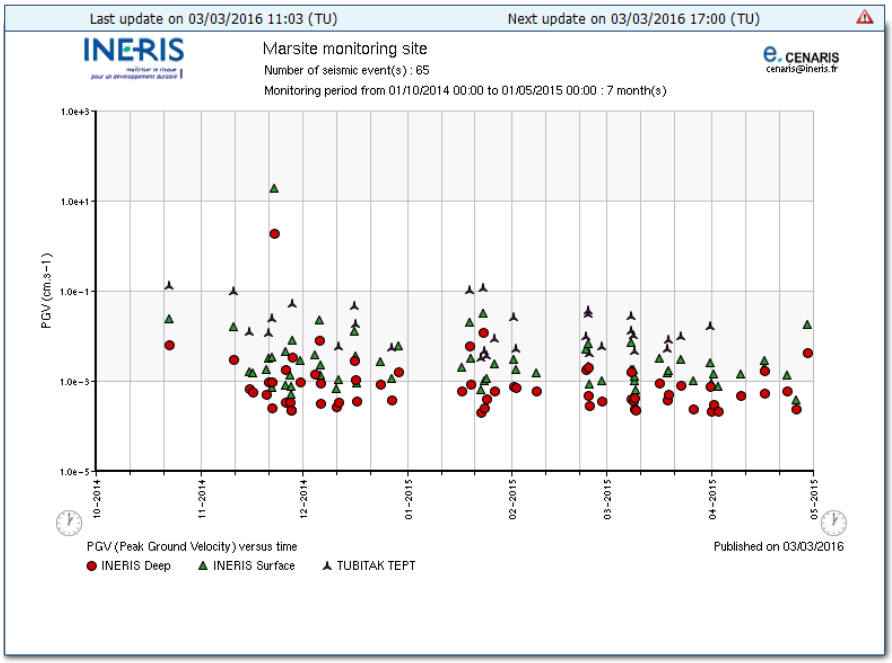

Figure 5: Peak Ground Velocity (PGV) versus time for INERIS deep and surface probes and the TEPT station.

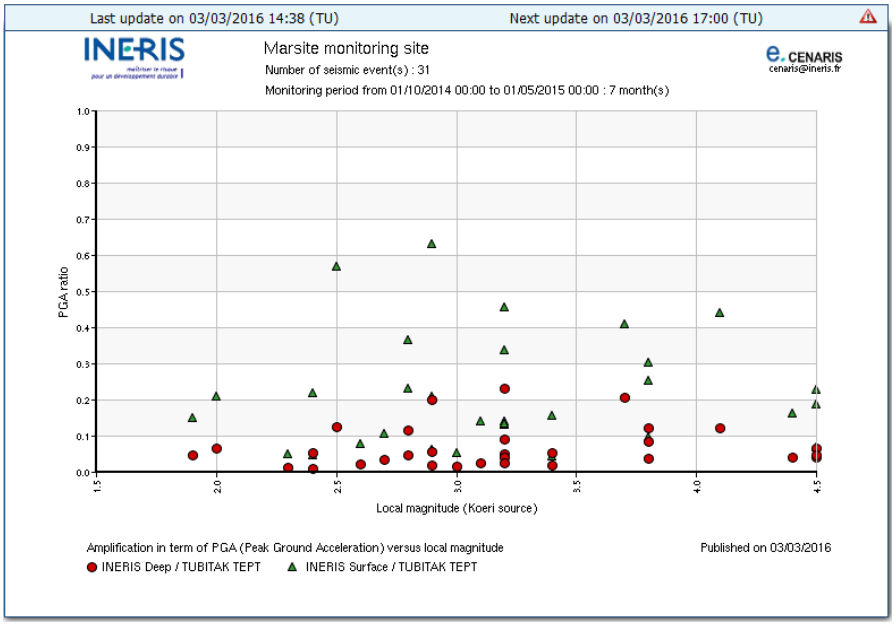

Figure 6: Amplification in term of PGA in %g versus local magnitude (source KOERI).

The collected meteorological records show piezometer trends related to seasonal as well to intense rainfalls (see Figure7). In addition, a rainfall data gap is present because of a cleaning problem of the weather station.

Concerning the moisture sensor, from its installation to the end of 2015 it recorded always a water content equal to 100% (Figure7). It is based on Time Domain Reflectometry (TDR) technology to accurately measure the water content of soil. What this means is that this sensor is a no hassle, no maintenance, long lasting, probe. The calibration of the sensor on the field was not easy task to undertake. Since the

transduction proposed by the manufacturer is a standard one for common soils, the measurement must be read carefully on the basis of its variation more than its absolute values. Measurement accuracy is not yielded by the manufacturer. Anyway, when plunged in a loose saturated soil the measurement value comes to 100%.

The collected geodetic data show a continuous EW movement of the landslide according to the GPS Farm station (see Figure 8). The other GPS station (House station) does not show any particular displacements demonstrating the complexity of the landslide movement (Figure 9).

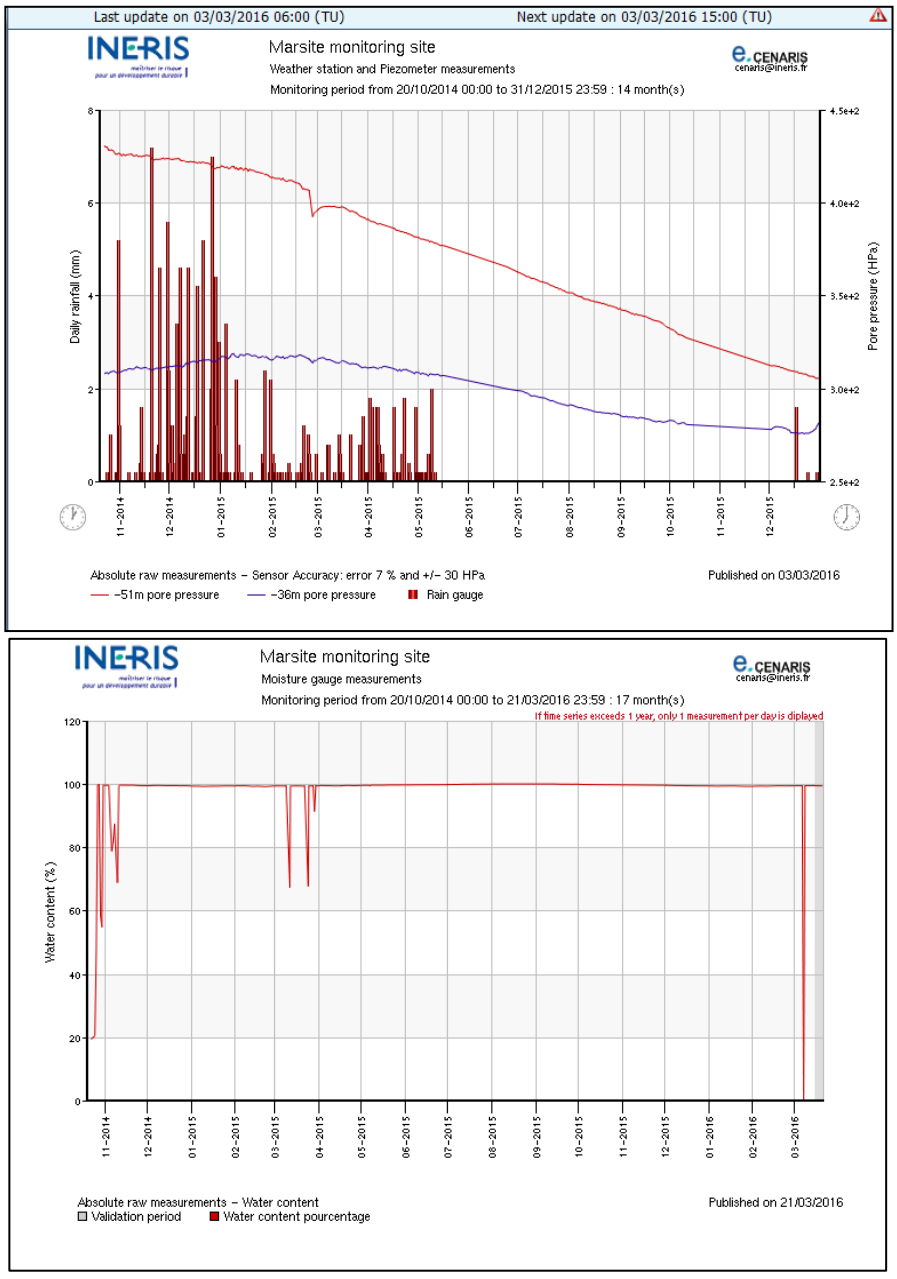

Figure7: Rainfall data and piezometer results on the top and below the water content.

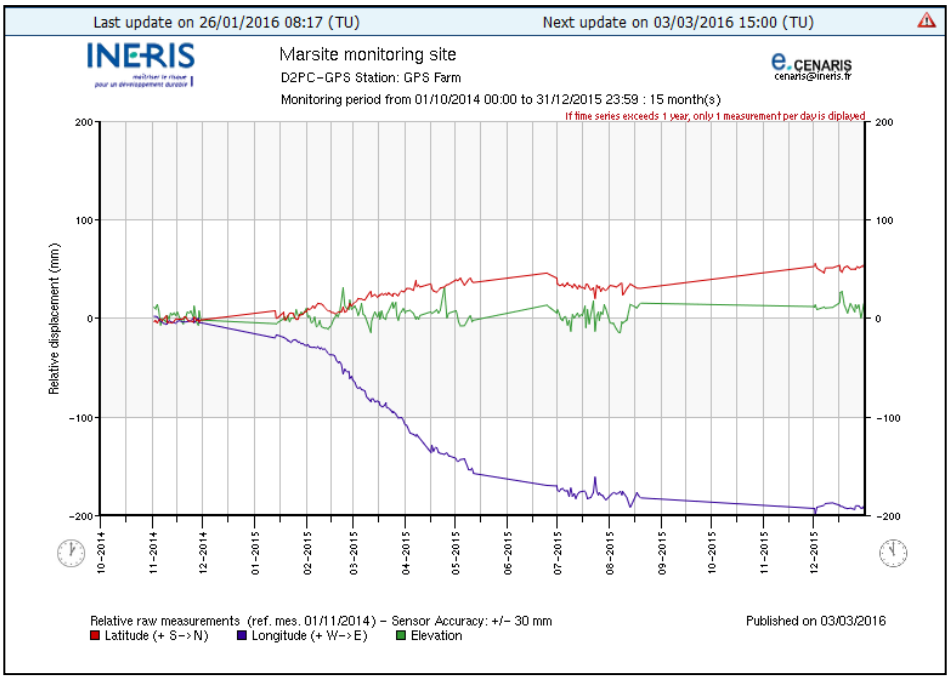

Figure 8: Surface displacements (mm) at the GPS Farm stations.

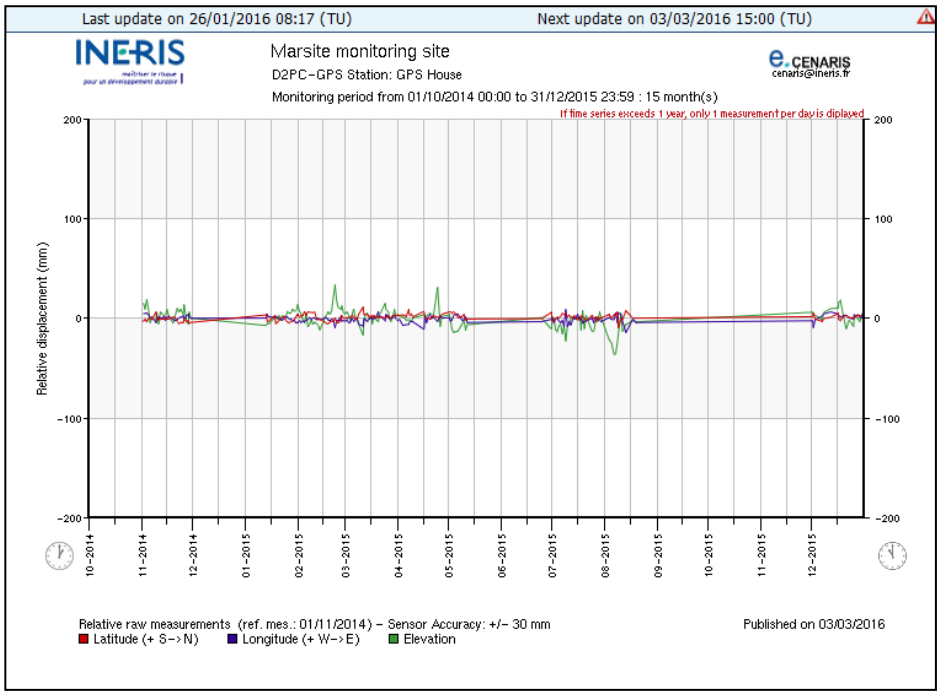

Figure 9: Surface displacements (mm) at the GPS house stations.

2.2 e-cenaris WEB MONITORING

The data recorded and processed by INERIS can be viewed and downloaded from the e-cenaris (http://cenaris.ineris.fr/). The site is open to the partners of the WP6 and WP9 project using only a “username” and a “password”. The newly recorded data are

transmitted several times a day and automatically integrated in the database management system of the e-cenaris infrastructure.

From the web monitoring desk, pre-defined graphics, tables and maps offer a easy-to-read and precise insight on the incoming dataset to make easier the understanding of the physical measurements, more accurate the interpretation and more efficient the decision making.

Most plots, tables and maps are easily exported to compile reports on line. It is possible to select and zoom any graphic, XY windows, display options, download any combination of freshly updated plots anytime and anywhere to build your own edition tasks easily. You can also force the page to update, edit and export easily raw and transformed data to complete further analysis with your own tools.

Documentation related to the project is accessible to share the information between the different partners involved.

In addition, the e-cenaris platform enables to cross-check seismic data in real time with the seismic catalogue of the Koeri web-page (http://www.koeri.boun.edu.tr/sismo/2/latest-earthquakes/list-of-latest-events/). In fact, the information about the localization, the local magnitude of the all earthquakes recorded by the local INERIS network comes from the Koeri web-page. The same cross-checking is possible with rainfall dataset available on a public web-page.

In complement to the time series visualization through e-cenaris, the implementation of an early warning tool has been designed, where the alarm may be transferred automatically to different authorities and partners with personalized notification message, was also carried out. To this purpose, the e-cenaris RDBMS (Remote Data Base Management System), fed in near to real time by the monitoring system in the field, has been interfaced with an advanced remote alarm management tool according to the following criteria:

- *simple alarm on time series*: alarm from a sensor measure (i.e.: piezometer pressure, number of earthquakes, etc.),
- *simple alarm on complex variables*: alarm from advanced processing of dataset (average value, ratio value, etc.). By “complex variable”, one must read processed and transformed data;
- *complex alarm*: operational alarm featuring data fusion approach, that is combination of relevant logical conditions (“and”, “or”, “not”) built on simple alarms (i.e.: rainfall and piezometer measurements, rainfall and GPS data, etc.).

2.3 Definition of a landslide warning system

Recall that the Cekmece-Avcilar peninsula is characterized by landslides, showing high susceptibility to both heavy rainfall and earthquakes. Therefore, an efficient early warning system has to take into account these two triggering factors.

Current probabilistic estimate of a major earthquake in Istanbul is about 2% per annum (Erdik et al, 2003). Concerning earthquake early warning (EEW), two approaches are possible: regional warning and on-site warning. The first is already existent in the Istanbul area and based on Turkish regional seismic networks (Erdik et al, 2003). Istanbul Earthquake Early Warning and Rapid Response System (IEEWRRS) has been deployed in 2002 by Kandilli Observatory and Earthquake Research Institute (KOERI). We focused on the second, based on individual sensors installed at the Büyükçekmece landslide. Generally, for on-site warning the beginning of the ground motion (mainly P waves) recorded at a site is used to predict the ensuring ground motion (S waves and surface waves) at the same site (Alcik et al, 2011).

From the scientific point of view one of the main problems still matter of debate was the forecasting of the magnitude of an earthquake based on the information given by the first 3 seconds of P-waves. Anyway, the most used parameters were the dominant

frequency (τc max), the average frequency (τc) or the peak displacement (Pd). The application to M>6 earthquakes was of major concern as the rock fracturing will still be in progress when the forecasting is done. (Allen and Kanamori, 2003; Kanamori, 2005; Wu and Kanamori, 2005).

Real-time rainfall data compared with rainfall thresholds can be incorporated into a landslide warning system. The effect of antecedent rainfall, and different rainfall intensity-duration schemes (short duration intense rainfall, prolonged low intensity rainfall etc.) have to be taken into consideration in evaluating the threshold critical rainfall that may trigger landslides at local or regional scales.

Anyway, the first simple factor to know is the total cumulative rainfall required for initiating slipping within the slope and then others characteristic indices of rainfall, such as duration, number of days a in a given period, etc...To obtain all these parameters long time-series of rainfall data are necessary.

The Marmara region in winter seasons sometimes receive heavy precipitation causing some floods and triggering landslides. The maximum daily precipitation recorded in the period of 1937-1990 varies between 43.8mm and 112.5mm (DMI, 1990). When 112.5 mm is considered, the maximum rainfall intensity is calculated as 4.7 mm/h. As a consequence, the region has the landslide triggers such as earthquake and heavy precipitation (Duman et al 2006).

3 Local site effects at Buyukcekmece landslide

Previous study on local site effects give evidence that the Avcilar district of western Istanbul (Özel et al., 2002; Tezcan et al., 2002) is characterized by the presence of soft sediments in basin structures and this has caused strong amplification of earthquake ground motion during past earthquakes. The alluvium, on the other hand, represents the most critical unit in terms of site amplifications and is limited to the fluvial depositional centres. The gentle topography of the area, with shallow synclines and anticlines plunging towards the Marmara Sea in the south, represents an environment significantly different from classical alluvial valleys or closed sedimentary basins. In this respect, the expected site effects also differ significantly (Sørensen et al., 2006).

Local site effects for the Buyukcekmece landslide were analyzed by using ambient noise data and earthquake data. The ambient noise data were recorded at 37 sites. The earthquake data were recorded by INERIS stations.

3.1 Noise data

The noise measurements were performed at 37 sites with a Guralp 6T velocitymeter sensor (Figure 10). The record durations were 50 minutes in general, but 24-hour records were obtained at 7 sites. A 5 % cosine taper was applied to each window and the Fourier spectra were calculated and smoothed through the Konno and Ohmachi (1998) algorithm, fixing the relevant parameter b to 20. The H/V values for each window were calculated as the ratio between the vector summation of the Fourier spectra of horizontal components and the spectrum of the vertical component. Lastly, thus obtained H/V curves were averaged out considering a log-normal distribution of amplitudes to obtain the mean H/V curve along with the relevant 68 % confidence interval. Windows exhibiting large transients were generally excluded from the analysis; these windows were visually identified from the velocity time series and from the single window Fourier spectra and spectral ratio.

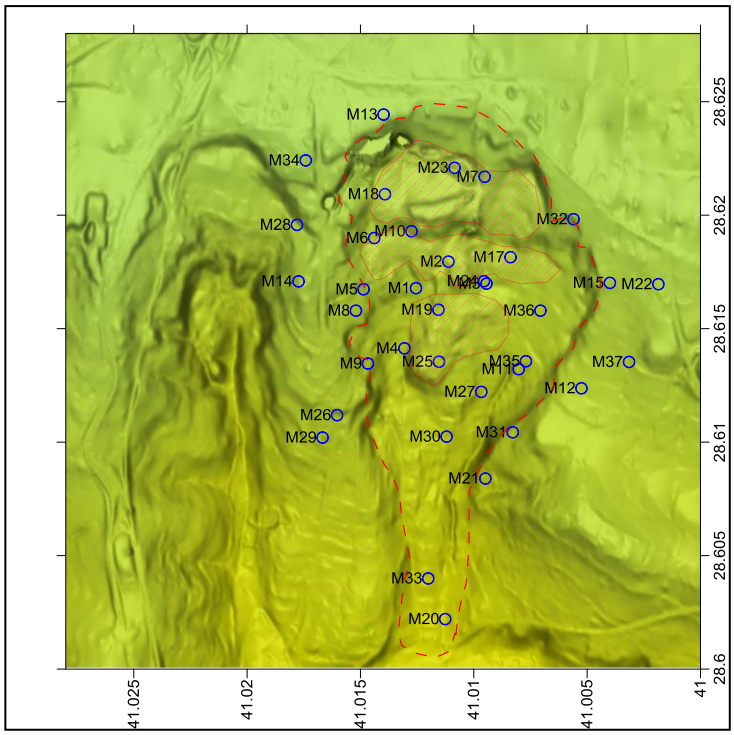

Figure 10: Locations of ambient noise measurements. Dashed red line represents the border of landslide.

Figure 11 shows the distribution of the site resonance frequencies obtained from the H/V analysis. It is to say that to decide resonance frequencies on the H/V curves was very difficult. One of the reasons of this is that the ambient noise records contain some anthropogenic vibrations, which are likely generated by industrial machines working in the region. The fundamental mode frequency of these vibrations is about 1.5 Hz, and they cause a false resonance frequency or they mask a real resonance frequency at some sites. In the analyses, we tried to keep away from the industrial peaks while determining the resonance peak of the H/V curve. Another reason is that a number of sites in our measurements do not present a clear resonance peak as defined in the SESAME project (Bard and SESAME Team, 2005). At these sites, the resonance frequencies were determined by comparing the H/V curves with those of neighboring sites showing clear peak.

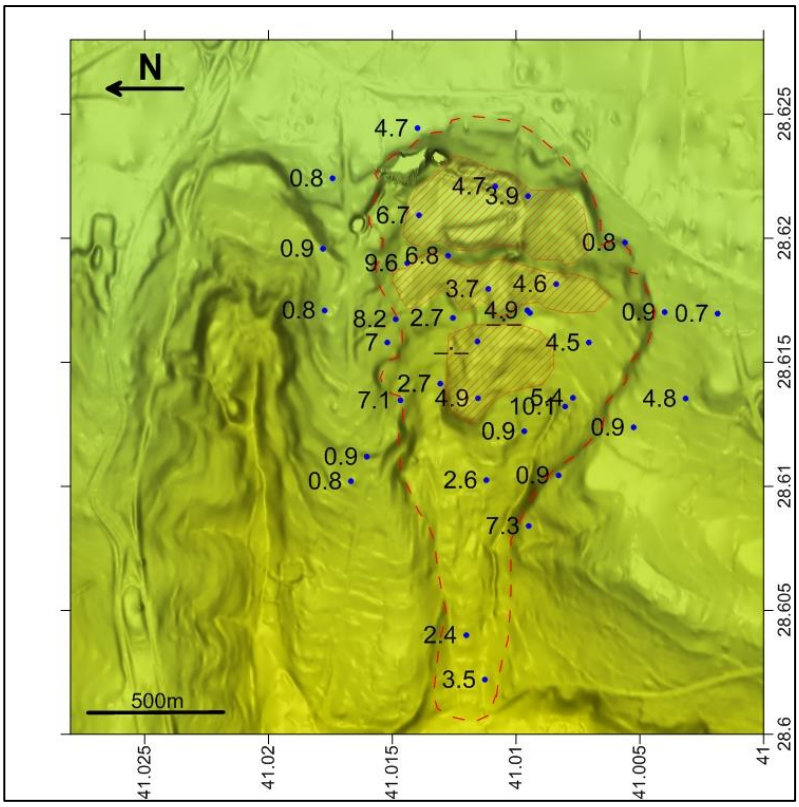

Figure 11: Site resonance frequencies obtained by H/V analysis.

The resonance frequencies determined under all these conditions are shown in Figure 11. It is seen that the resonance frequencies on the sliding mass are generally higher than those placed outside of landslide. In the middle of sliding mass resonance frequencies are between 2.7-4.9 Hz (Figure 12), whereas at the sites surrounding the landslide area the values decrease to 0.7-0.9 Hz (Figure 13). At some transition sites, high resonance frequencies of 6-10 Hz are also observed (Figure 14).

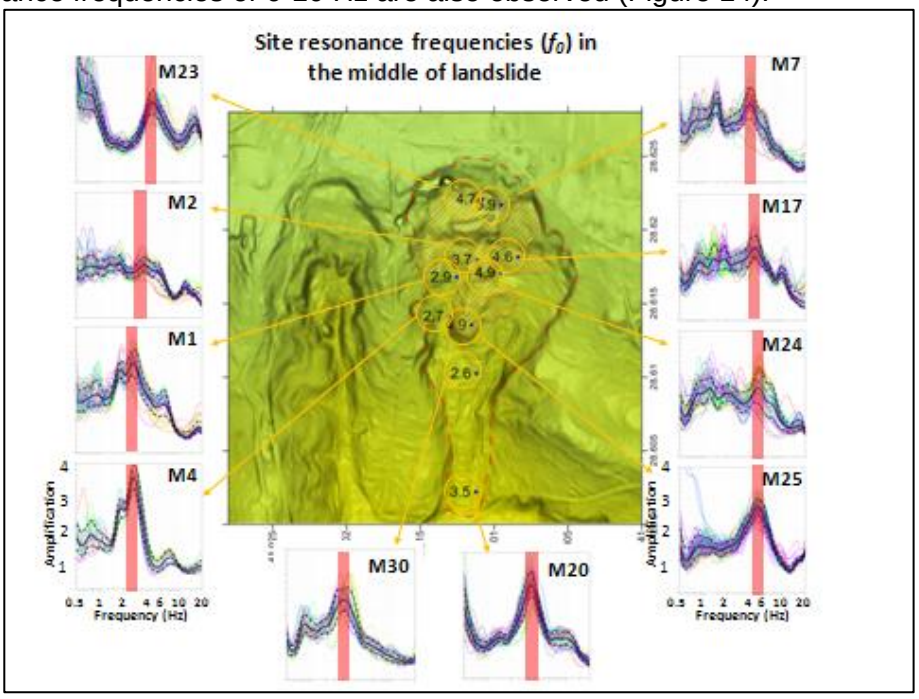

Figure 12: H/V curves and site resonance frequencies (red bars) at the sites located on the landslide area.

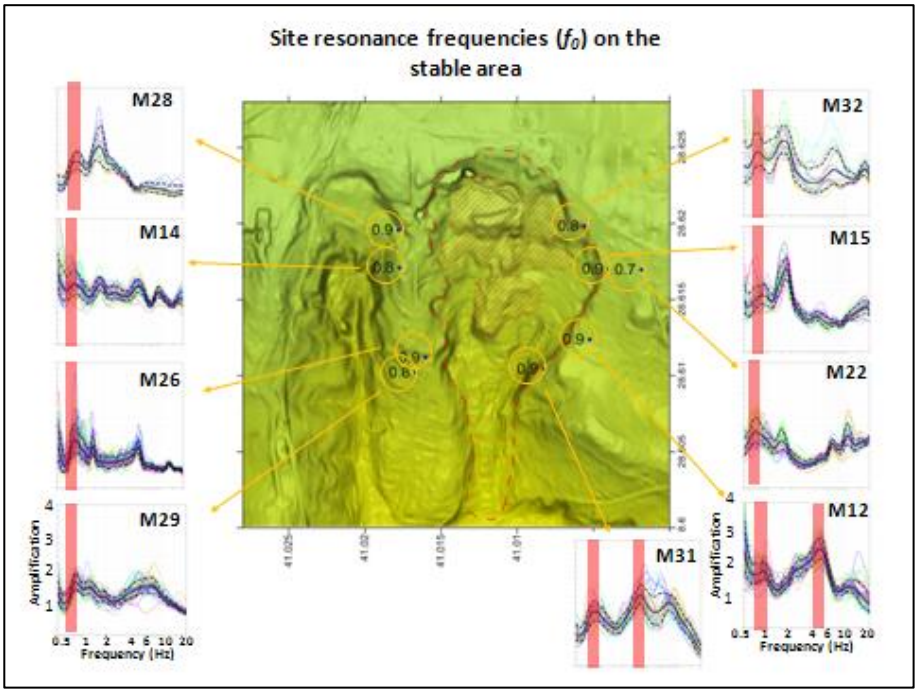

Figure 13: H/V curves and site resonance frequencies (red bars) at the sites located on the stable area.

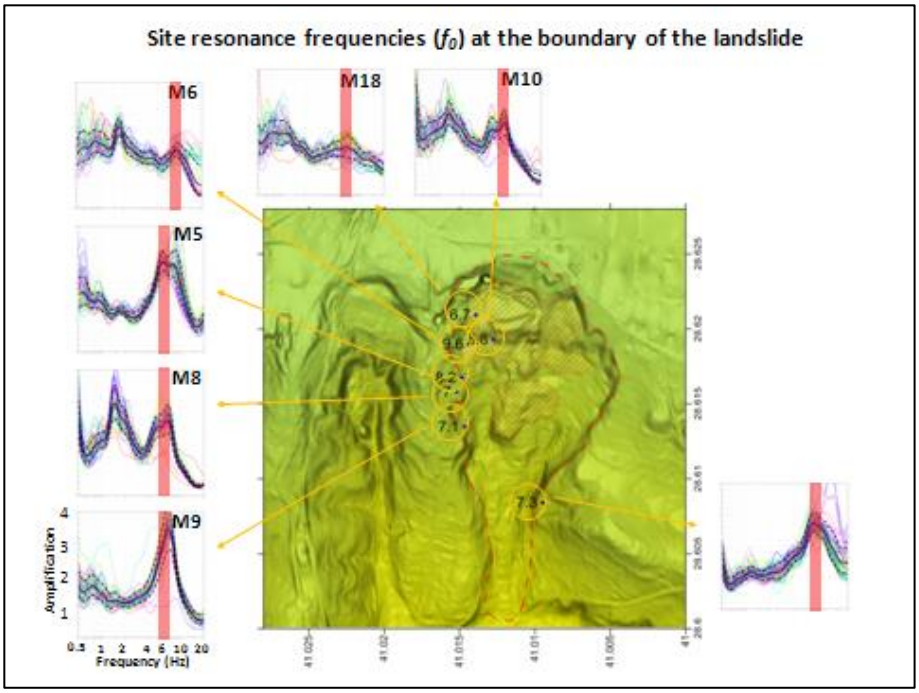

Figure 14: H/V curves and site resonance frequencies (red bars) at the sites located on the transition region between landslide and stable areas.

The resonance frequencies (*fr*) of the H/V curves can be converted to soil thicknesses (*H*) by using empirical relations. Birgoren et al. (2009) suggests a relationship ($\mathrm{H} = 150.99\mathrm{f_r}^{-1.1531}$) between soil thickness and resonance frequency for the Istanbul

region. The soil thicknesses computed from the Birgoren's empirical relation are shown in the Figure 15. It is seen that the soil thicknesses in the middle part of the landslide – the thicknesses of the sliding mass to be more precise – range from 17 to 50 m, and from 10 to 17 m on the edges of the landslide. The soil thickness on stable part – we use this time the term of soil thickness by assuming that the actual soil generate resonance vibration– reaches to 170-228 m which likely points out a lithological change in deeper sediments.

We have a borehole section provided by TUBITAK on the landslide area. Figure 15 gives the borehole section, too. As seen in the section, two failure surfaces have been cut by the borehole. The depths of the sliding surfaces are about at 30 m and at 50 m, which are not so different from the depths obtained by the resonance frequencies.

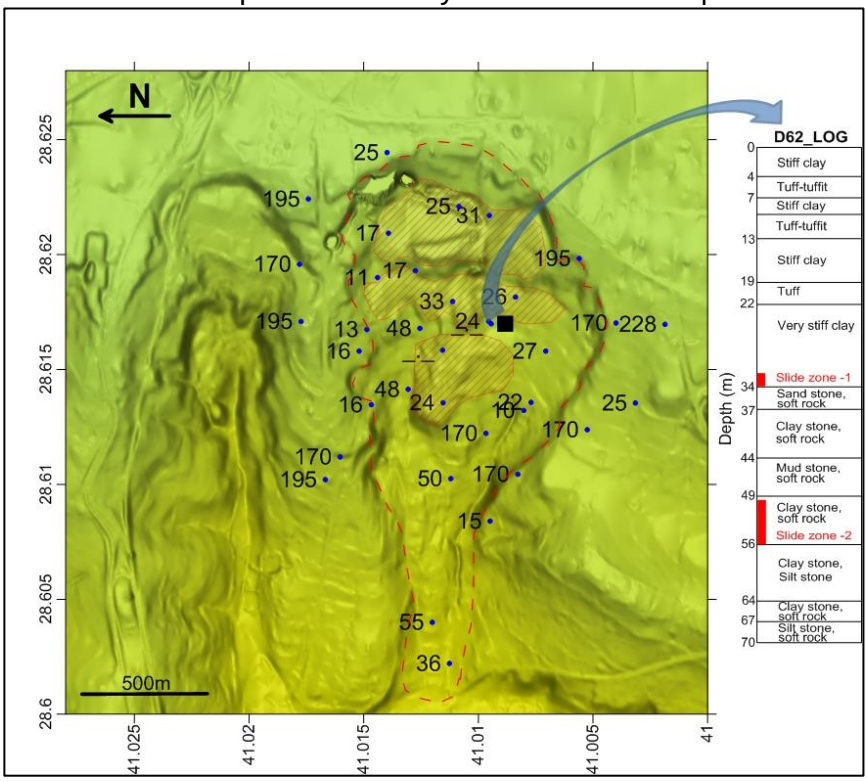

Figure 15: Soil thicknesses computed from resonance frequencies by the empirical relation of Birgoren et al. (2009). It is also shown a lithological section obtained from a borehole whose location is shown with square on the map.

3.2 Earthquake data

We computed several spectral ratios by using 45 earthquake data recorded by INERIS network, which they include surface horizontal-to-vertical ratio, downhole horizontal-to-vertical ratio, surface horizontal-to-downhole horizontal ratio and finally surface vertical-to-downhole vertical ratio. It is used 20 events in computing each spectral ratio, which is sufficient to obtain a reliable result. Firstly, S-waves are manually windowed from three components with a length of approximately 10 s, and then their Fourier spectra are computed. The spectra are smoothed with a Konno-Ohmachi operator with b value of 40. Average horizontal component (H) is computed from two horizontal components by using root mean square. Finally, spectral ratios are computed for each event and then the mean ratio is computed by geometric average.

We should express that the records of downhole station includes down-going waves reflected from the surface together with up-going waves. Therefore, it is likely that the spectral ratios computed by downhole records contain destructive and constructive effects of down-going waves.

Figure 16 shows the horizontal-to-vertical spectral ratios at the surface and downhole stations. The horizontal-to vertical spectral ratios show significant scattering at the frequencies below 2 Hz, so it is not possible to obtain a reliable result especially at low frequencies. H/V ratios at downhole station exhibit many peaks at nearly 3, 5.5 and 10.5 Hz. H/V ratios of surface station present a sharp peak at 1.5 Hz, and show amplification in a broad band between 3 and 10 Hz.

Figure 17 shows surface-to-downhole ratios for horizontal and vertical components. The horizontal component ratios of surface and downhole stations are highly concentrated and the peaks are clear, contrary to the vertical component ratios. At this stage, it is not clear which peaks on the spectral ratios are caused by interference of down-going and up-going waves.

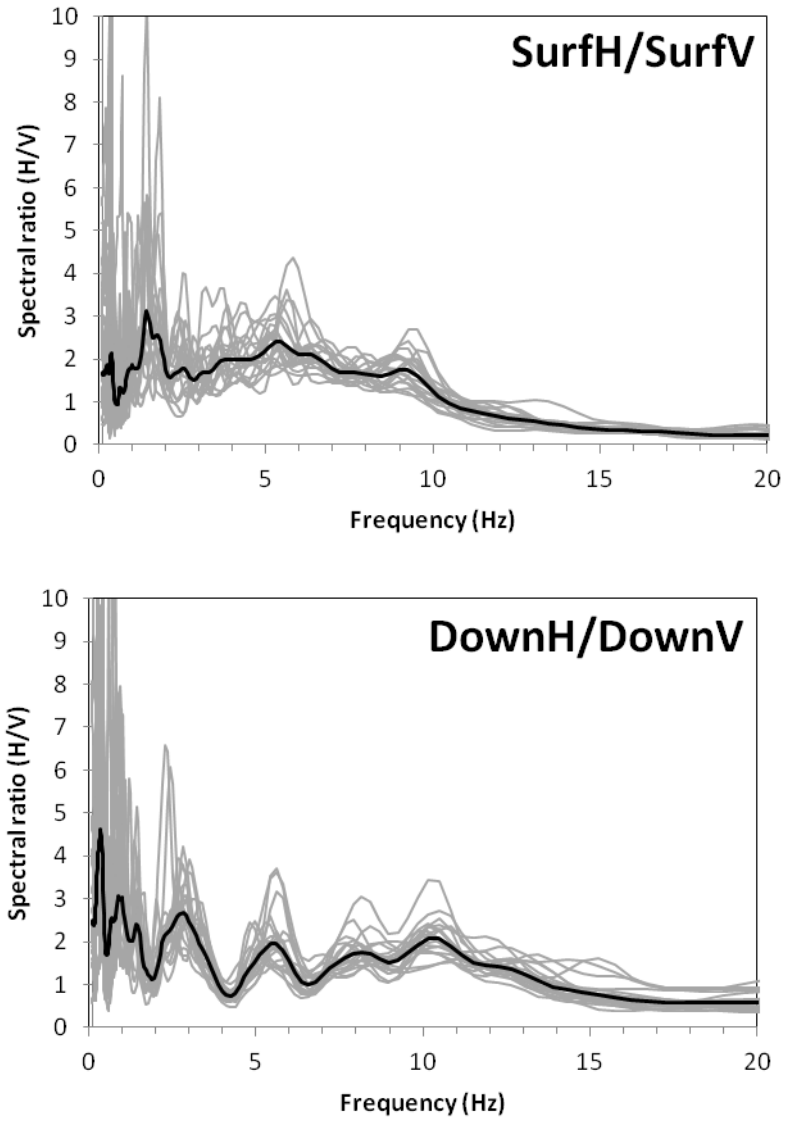

Figure 16: Horizontal-to-vertical spectral ratios at the surface station (upper graph) and downhole station (bottom graph). Grey and black lines represent ratios for each event and average, respectively.

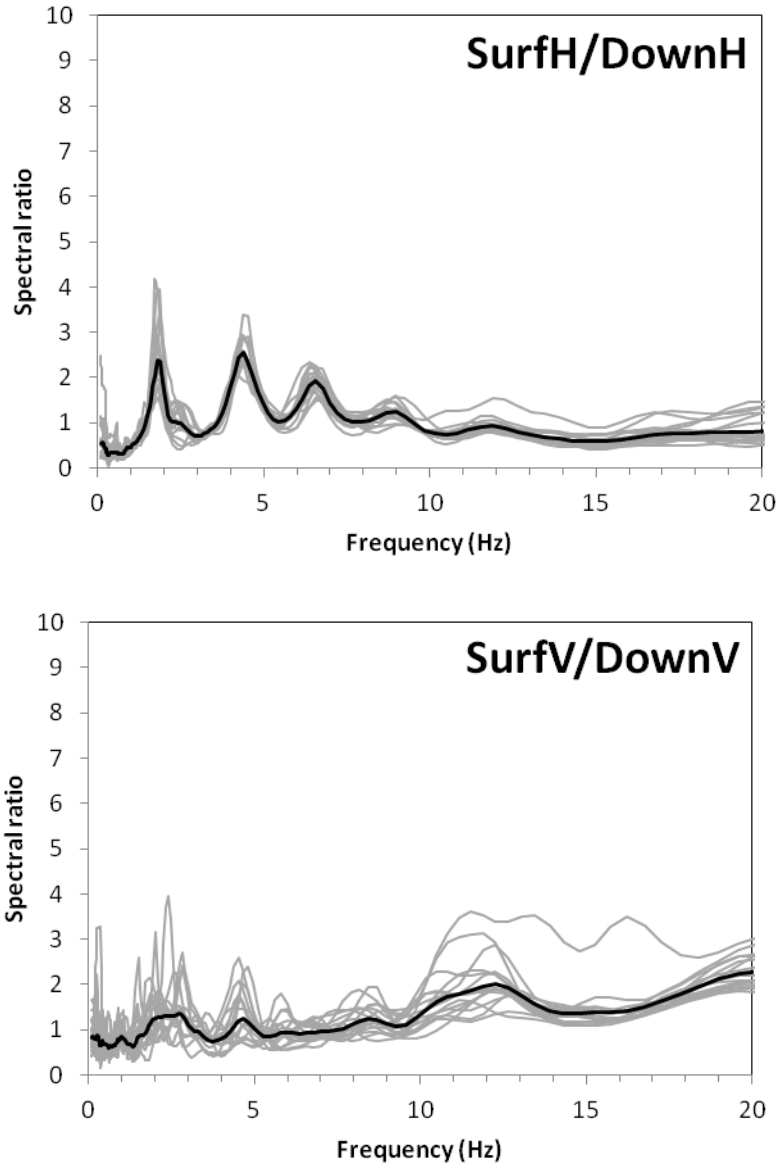

Figure 17: Spectral ratios of surface horizontal-to-downhole horizontal components (upper graph) and surface vertical-to-downhole vertical components (bottom graph). Grey and black lines represent ratios for each event and average, respectively.

4 Numerical modeling

IFSTTAR-La Sapienza worked on the restitution of the collected data on a WebGIS geodatabase, the processing and analysis of the recorded earthquakes and the numerical modelling of the local seismic response and the expected earthquake-induced displacements in the Büyükçekmece landslide area.

4.1 Data collection and WebGIS geodatabase construction

Data derived from engineering-geological field surveys and geophysical investigations carried out in the Büyükçekmece landslide area during the MARsite project in the framework of the WP6b activities, as well as the locations of the earthquakes recorded by the INERIS seismic probes were used to create a geodatabase that was implemented on-line on a WebGIS platform (licence of CERI-Sapienza).

This geodatabase (Figure 18) is now available for all the WP6 MARsite partners at the web-site http://www.ceri.uniroma1.it/cn/index.do?id=1000&page=1000 to share maps, data and information, useful for engineering-geological modelling and numerical simulations. Part of the results obtained from data processing is also reported in specific layers. The WebGIS manages a user-friendly multi layers interface for consulting the geodatabase, allowing to select some of the info-layers and to plot them on a base map that can be selected among different solutions (satellite view, road map, etc). The info points can be queried by pop-up windows that include the collected/analyzed/processed info-data. In the following, examples of queries and corresponding pop-up windows are presented.

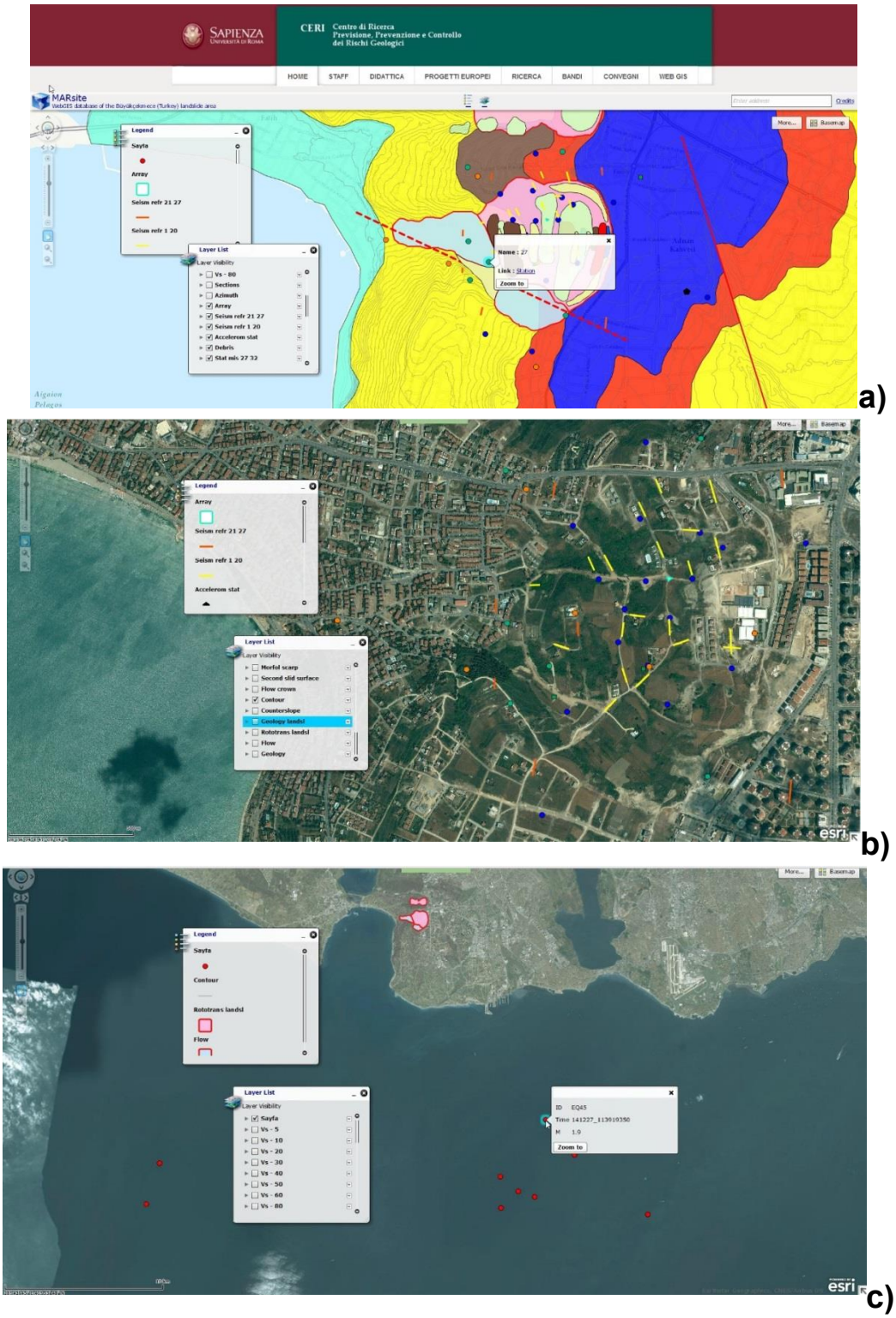

Figure 18: examples of WebGIS masks available on-line at the web site http://www.ceri.uniroma1.it/cn/index.do?id=1000&page=1000. From the top to the bottom: a) geology of the landslide slope with location of geophysical investigations; b) satellite view of the landslide area with location of geophysical investigations; c) landslide location and epicenters of the recorded earthquakes.

4.2 Processing of the recorded earthquakes

The characteristics and locations of the 45 recorded earthquakes are reported in Table 1 and Figure 19. These data were considered to assess the local seismic response of the Büyükçekmece landslide in terms of amplifications and to define the transfer function associated to the INERIS 3-components seismic probes. The earthquake records were also collected by the velocimetric station (TEPT) managed by the TUBITAK.

Table 1: Earthquakes recorded at MARsite and TEPT (TUBITAK) station during the project

	Location	Lat	Long	M	TEPT station	MARSite stations
EQ1	ROMANYAQuick	45.742	27.2147	5.6	142211_1900_TEPT.1	141122_19152261
EQ2	AEGEANSEAQuick	38.8942	26.2723	5.1	141206_0130_TEPT.1	141206_01453288
EQ3	PAMUKOVAQuick	40.4047	30.1188	4.5	22-1711-05L.S201410_TEPT.1	141022_171122806
EQ4	SIMAV (KUTAHYA)	39.3512	29.018	4.5	142811_0230_TEPT.1	141128_023032650
EQ5	UGURLUPINAR-MUSTAFAKEMALPASA (BURSA)	40.0647	28.587	4.5	23-1019-43L.S201501_TEPT.1	150123_101942108
EQ6	SAKIZADASI (AEGEANSEA)Quick	38.6145	26.1205	4.4	141204_2100_TEPT.1	141204_21171928
EQ7	CELTIK-BIGA (CANAKKALE)Quick	40.1478	27.0735	4.4	16-0902-14L.S201412_TEPT.1	141216_090222019
EQ8	SUDOSEGI-SIMAV	39.3408	29.0512	4.1	142611_0005_TEPT.1	141126_00051528
EQ9	AEGEANSEAQuick	38.899	26.2262	4.1	141206_0830_TEPT.1	141206_08372110
EQ10	SAROS KORFEZI (AEGEAN SEA)	40.3412	26.0567	4.1	02-0441-03L.S201502_TEPT.1	150202_044133116
EQ11	AEGEANSEAQuick	40.2098	25.2578	4	142711_1200_TEPT.1	141127_122018572
EQ12	SIMAV (KUTAHYA)	39.3487	29.0332	3.9	143011_0630_TEPT.1	141130_063856860
EQ13	SIMAV	39.3422	29.032	3.8	141115_0730_TEPT.1	141115_073041776
EQ14	SIMAV	39.3468	29.0128	3.8	141611_0830_TEPT.1	141116_084348663
EQ15	KABAKDERE-(BALIKESIR)	39.663	27.8603	3.8	23-0053-11L.S201502_TEPT.1	150223_005319587
EQ16	KABAKDERE-(BALIKESIR)	39.6697	27.8405	3.8	19-0648-57L.S201503_TEPT.1	150319_064907179
EQ17	BALIKESIR	39.644	27.8502	3.7	18-2050-01L.S201503_TEPT.1	150318_205011889
EQ18	BERGAMA (IZMIR)	39.3172	27.0518	3.6	142211_0000_TEPT.1	141122_001214945
EQ19	SIMAV	39.3575	29.0008	3.5	142611_0012_TEPT.1	141126_001206084
EQ20	SIMAV (KUTAHYA)	39.3448	29.0292	3.5	142711_2030_TEPT.1	141127_20370998
EQ21	SAROSKORFEZI (AEGEANSEA)Quick	40.4917	26.3838	3.5	141206_1200_TEPT.1	141206_120800592
EQ22	GUZELKOY ACIKLARI-TEKIRDAG (MARMARA SEA)	40.7125	27.4973	3.5	01-1046-31L.S201502_TEPT.1	150201_104633047
EQ23	AKTARMA-(BALIKESIR)	39.7248	27.7733	3.4	27-1240-17L.S201502_TEPT.1	150227_124031985
EQ24	GORDES (MANISA)	38.8595	28.1088	3.3	142711_1500_TEPT.1	141127_150719665
EQ25	MARMARASEAQuick	40.8433	28.7897	3.2	10-1824-48L.S201411_TEPT.1	141110_182446008
EQ26	KAYNARCA-BIGA	40.1008	27.2618	3.2	142011_1330_TEPT.1	141120_133922701
EQ27	ARMUTLU (YALOVA)[NORTHEAST8.7KM]Quick	40.596	28.848	3.2	16-1926-33L.S201412_TEPT.1	141216_192624220
EQ28	SOGUTALAN-MUSTAFAKEMALPASA (BURSA)	40.0558	28.571	3.2	26-1708-27L.S201501_TEPT.1	150126_170828619
EQ29	KABAKDERE-(BALIKESIR)	39.6688	27.8653	3.2	23-1743-39L.S201502_TEPT.1	150223_174410094
EQ30	ERDEK KORFEZI (MARMARA SEA)	40.3705	27.6472	3.2	08-1805-24L.S201503_TEPT.1	150308_180523430
EQ31	ERDEK ACIKLARI-BALIKESIR (MARMARA SEA)	40.6097	27.817	3.1	31-1516-56L.S201503_TEPT.1	150331_151643312
EQ32	MARMARA SEA	40.8648	28.6787	3	19-1110-43L.S201501_TEPT.1	150119_111029408
EQ33	MARMARASEAQuick	40.8545	28.2947	2.9	22-0556-30L.S201411_TEPT.1	141122_055632570
EQ34	ESENKOY-CINARCIK (YALOVA)Quick	40.5978	28.8527	2.9	11-1628-21L.S201412_TEPT.1	141211_162818745
EQ35	INCEALIPINAR-MUSTAFAKEMALPASA (BURSA)	40.0827	28.5975	2.9	24-1541-24L.S201501_TEPT.1	150124_154139730
EQ36	INCEALIPINAR-MUSTAFAKEMALPASA (BURSA)	40.0707	28.5985	2.8	23-1744-57L.S201501_TEPT.1	150123_174511374
EQ37	MARMARA SEA	40.8565	28.6922	2.8	08-0916-53L.S201503_TEPT.1	150308_091637713
EQ38	MARMARASEAQuick	40.8262	28.119	2.7	21-0218-43L.S201411_TEPT.1	141121_021846046
EQ39	MARMARA SEA	40.8492	28.4123	2.6	23-1241-55L.S201502_TEPT.1	150223_124141352
EQ40	CINARCIK (YALOVA)	40.6233	29.1082	2.5	22-1647-04L.S201501_TEPT.1	150122_164703990
EQ41	AVCILAR (ISTANBUL)	40.8772	28.7345	2.4	08-0227-08L.S201503_TEPT.1	150308_022653546
EQ42	MARMARA SEA	40.847	28.6792	2.4	22-1948-21L.S201503_TEPT.1	150322_194807211
EQ43	MARMARA SEA	40.8725	28.4223	2.3	23-1237-50L.S201502_TEPT.1	150223_123741203
EQ44	MARMARA SEA	40.8533	28.7045	2	09-0226-44L.S201503_TEPT.1	150309_022633615
EQ45	AVCILAR (ISTANBUL)Quick	40.8972	28.7128	1.9	27-1139-30L.S201412_TEPT.1	141227_113919350

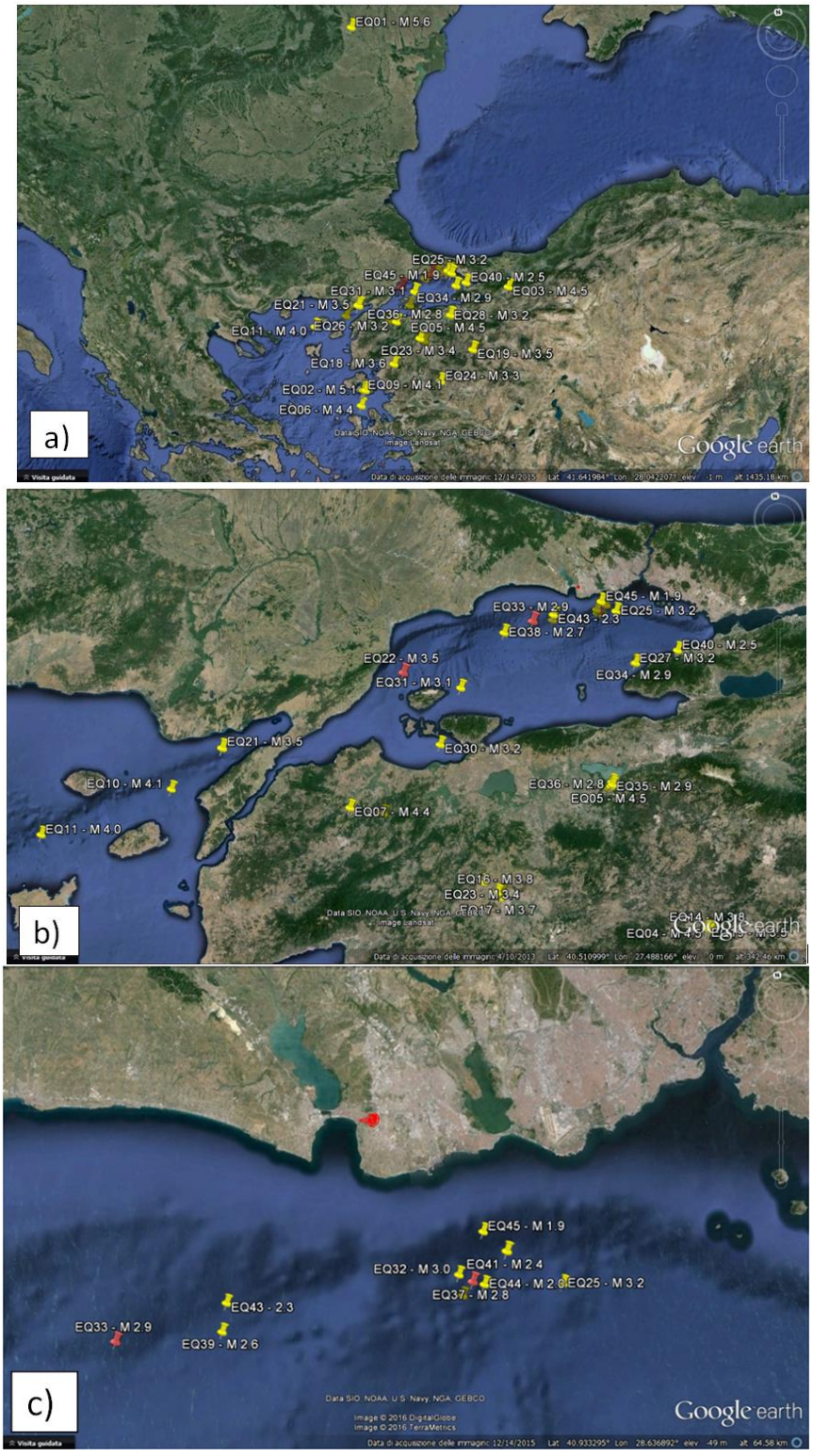

Figure 19 : Locations of the earthquakes recorded at MARsite and TEPT stations during the project. The red pointers highlight the earthquakes used for the numerical modelling of the local seismic response of the Büyükçekmece landslide. The zoomed satellite views refer to the continental area (a); the Marmara sea region (b) and the Avcilar peninsula (c) respectively. The Büyükçekmece landslide is also reported (red filled hatch).

Some preliminary analyses were performed on the earthquakes records to derive the distributions of Arias Intensity (AI) vs PGA (Peak Ground Acceleration) values on the

one hand and earthquakes characteristic periods (Tm) vs. AI on the other hand. The results are reported on Figure 20 for MARsite and TEPT stations considering the two horizontal components separately.

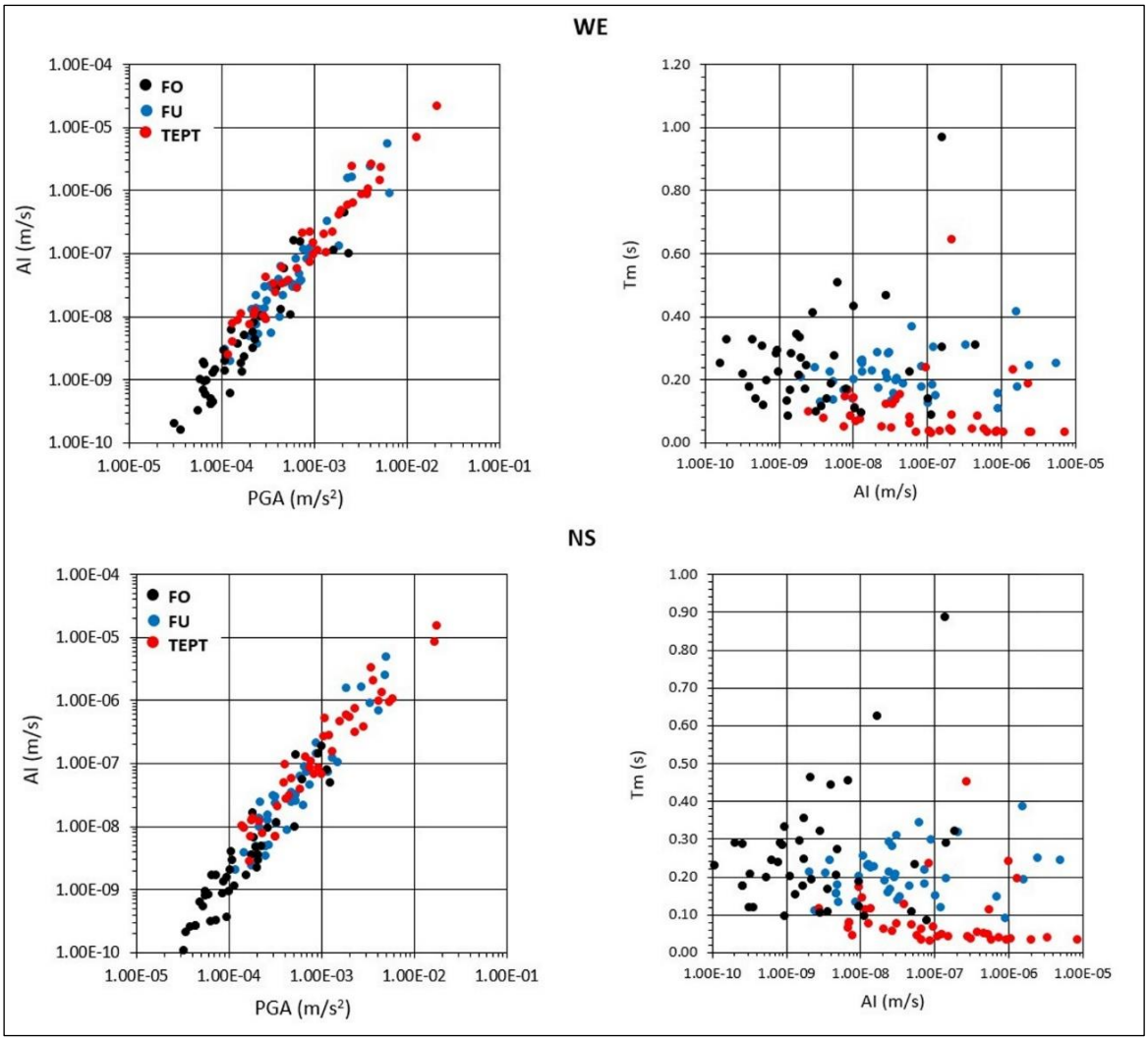

Figure 20 : AI vs. PGA and T_m vs. AI distributions for the earthquakes recorded during the project at MARSite (SU and FO) and TEPT stations. The two geographically oriented horizontal components (WE and NS) are shown.

According to TUBITAK, TEPT is a reference station located outside from the landslide area on stiffer soils. We checked this statement on our set of data calculating the associated mean H/V ratio.

The mean H/V spectral ratio (HVSR) for TEPT station was calculated considering the following steps:

1. time histories were cut to isolate the earthquakes from the rest of the signals;
2. all processed signals were rotated to derive the movement along the principal direction of sliding of the landslide (E-W) and along the orthogonal direction (N-S);
3. signals were band-pass filtered between 0.1Hz-40Hz to avoid effect of long-period terms (removing of drifts) due to the instrumental response of the sensors (Butterworth 4 poles and 2 passages);
4. the Fast Fourier Transforms (FFTs) were computed for each earthquake in terms of amplitude and phase;

5. the FFT amplitudes were smoothed considering a frequency window of 0.5 Hz;
6. the HVSR were computed considering separately the two horizontal components (N-S and W-E oriented);
7. mean and standard deviation of HVSRs were computed by averaging the NS and WE components of the ground motion.
8. The conclusion is that TEPT station does not exhibit any amplification (Figure 21). It can therefore be considered as a true reference site based on our data set.

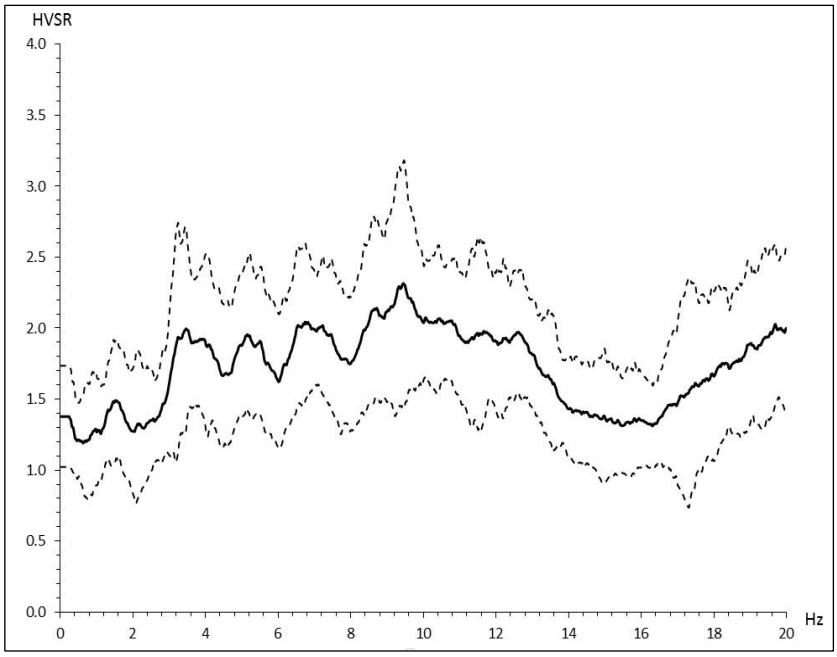

Figure 21 : average HVSR (continuous line) ± standard deviation (dashed lines) obtained for the earthquakes recorded at TEPT station during the MARSite project.

Additional data processing was performed on this set of data:
- Site-to-reference spectral ratios (SSR) at the borehole station (SU/TEPT) were computed considering all the recorded ground motion components.
- Empirical transfer functions which characterize the soil column representative for the landslide mass at the MARsite borehole site were also assessed considering the acceleration recorded at SU and FO stations. To compute these transfer functions, the following procedure was adopted:

1. acceleration time histories were transformed from counts to physical units using the zeroes-poles functions of the installed accelerometers;
2. acceleration time histories were cut to isolate earthquakes from the rest of the seismic signals;
3. all the acceleration time histories were rotated to deduce the movement along the principal sliding direction of the landslide (almost E-W oriented) and along the normal direction (N-S);
4. FFTs were band-pass filtered between 0.1Hz-40Hz to avoid effect of long-period terms (removing of drifts) due to the instrumental response of the sensors (Butterworth 4 poles and 2 passages);
5. the FFTs were computed in terms of amplitude and phase for each earthquake;
6. the FFT amplitudes were smoothed considering a frequency window of 0.5 Hz;
7. spectral ratios SU/FO were computed for each ground motion direction (i.e., N-S, W-E and Z);
8. mean and standard deviation were computed for the SU/FO spectral ratios.

The amplification at SU station was assessed based on the SU/FO spectral ratios computed at point 7) of the above listed procedure. The resulting amplification (Figure 22) shows values higher than 2 (up to 4) in a broad band of frequencies, between 1Hz and 8Hz, for all the components of the ground motion. These empirical outputs were compared with the numerical modelling outputs.
To this aim, 3 among the 45 recorded earthquakes (see red markers in Figure 19) were applied as inputs in the numerical modelling. They have been chosen based on the following characteristics: their location along the North Anatolian Fault Zone (NAFZ) at different distances from the landslide site (10, 50 and 100Km) and their spectra (shown on Figure 23) laying in the statistically significant range of all the FFTs computed for the 45 recorded earthquakes.

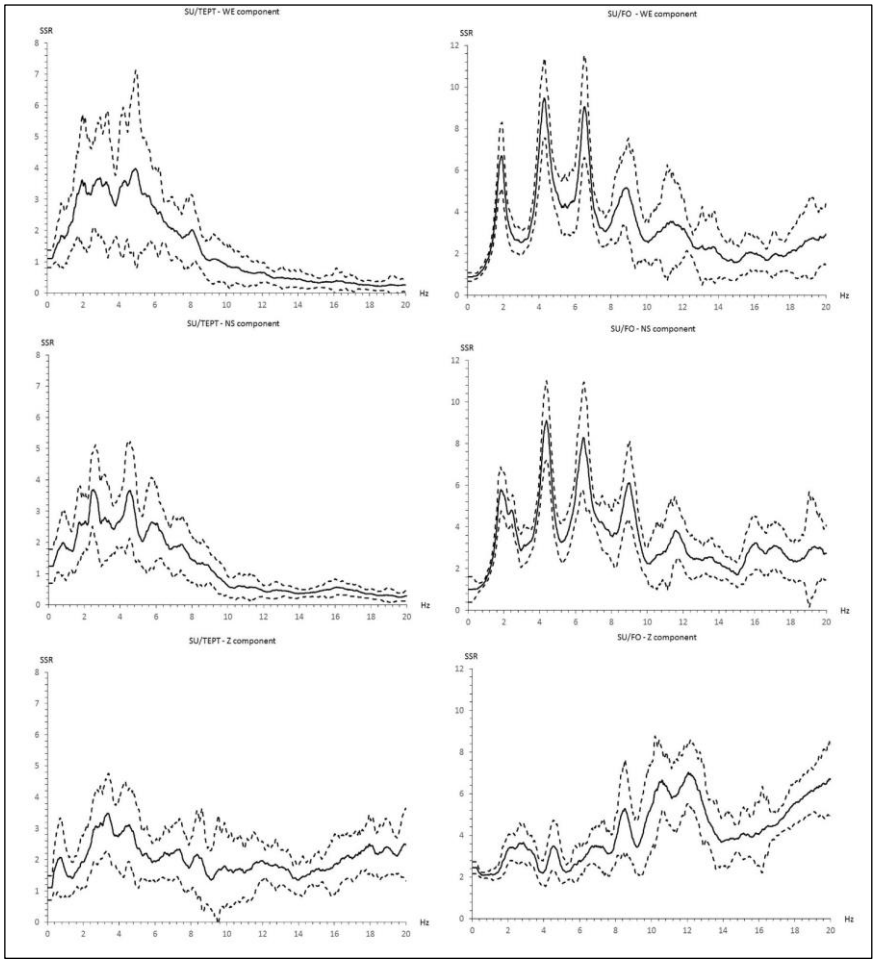

Figure 22: average SSR (continuous line) ± standard deviation (dashed lines) obtained for the earthquakes recorded at MARsite (SU and FO) and TEPT stations during the project.

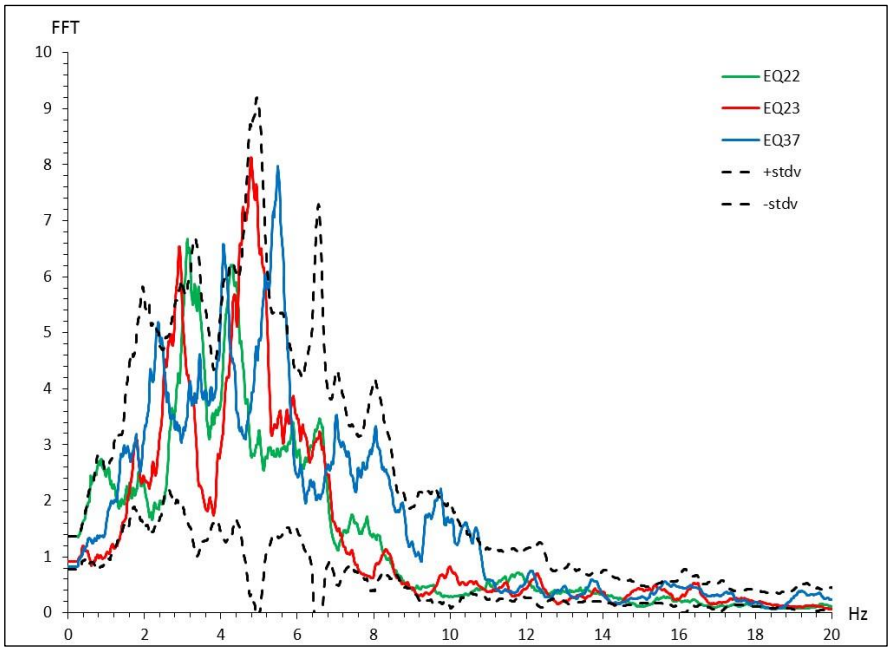

Figure 23 : FFTs amplitudes of the earthquakes selected for the numerical modelling (see Figure 19 for their epicentral locations). The standard deviation (dashed lines) for the average FFT from the 45 recorded earthquakes is also shown.

4.3 Numerical modeling of the local seismic response

In the framework of the MARsite project, we investigated the most hazardous landslide of the area, namely the Büyükçekmece landslide which can be described as an active retrogressive rototranslational landslide with a very complex lithological structure composed of several dislodged and counter-slope dipping blocks. The extensive field geological investigations, the geophysical measurements and boreholes stratigraphic logs as well as a literature review (Dalgiç, 2004; Duman et al. 2006) were combined to obtain a high-resolution engineering-geological model of the landslide identifying several lithological units, characterized by specific mechanical properties (see previous deliverable D6.1).

The landslide is composed of four main geological units (from the bottom to the top): silty clays (stable bedrock), clays with tuffs, sands and gravels and calcarenites. The toe of the landslide hosts an earthflow whose material is strongly remolded and poorly constrained. Refer to deliverable D6.1 for more details on this engineering-geological model and the physical and mechanical properties of each material used for the numerical simulations.

This landslide is located only 15km north from the NAFZ in an area where urbanization is growing very fast despite the presence of large pre-existing landslides. Figure 24 depicts the geological map of the Büyükçekmece landslide area and the 5 cross-sections considered for the numerical modeling are shown in Figure 25.

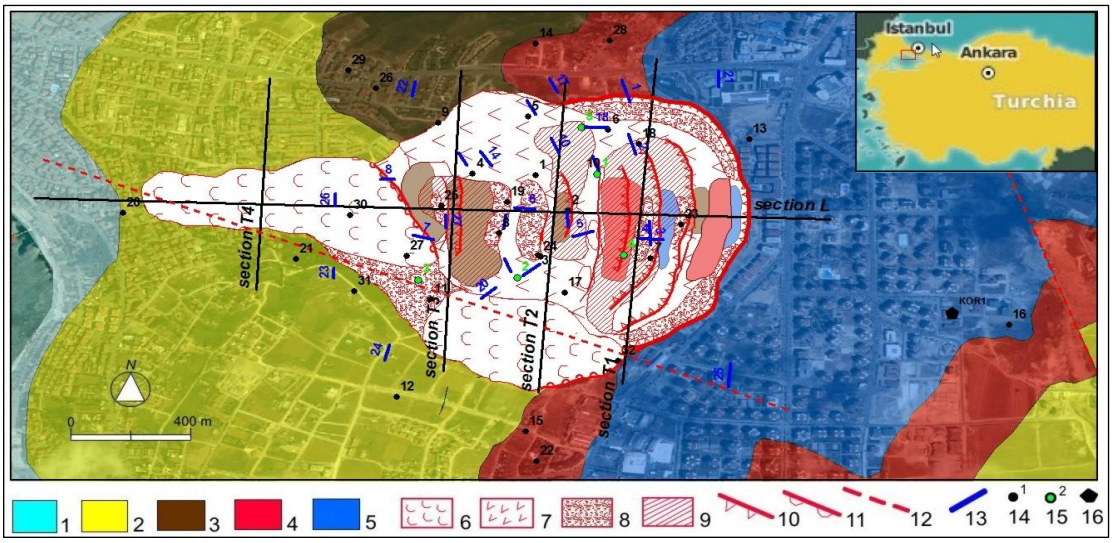

Figure 24: Geological map of the Büyükçekmece landslide area: 1) alluvial and coastal deposits (Holocene); 2) silty-clays of the Danisment Formation (upper Oligocene); 3) clays with tuffs for the Danisment Formation (upper Oligocene- lower Miocene); 4) sands and gravels of the Istanbul Formation - Kiraç member (upper Oligocene- lower Miocene); 5) calcarenites of the Çekmece Formation - Bakirköy member (upper Miocene); 6) earthflow debris; 7) rototranslational landslide mass; 8) slope debris; 9) landslide counterslope tilted terrace; 10) rototranslational landslide scarp; 11) earthflow crown; 12) fault; 13) seismic lines; 14) noise measurement station; 15) VES measurement point; 16) accelerometric station.

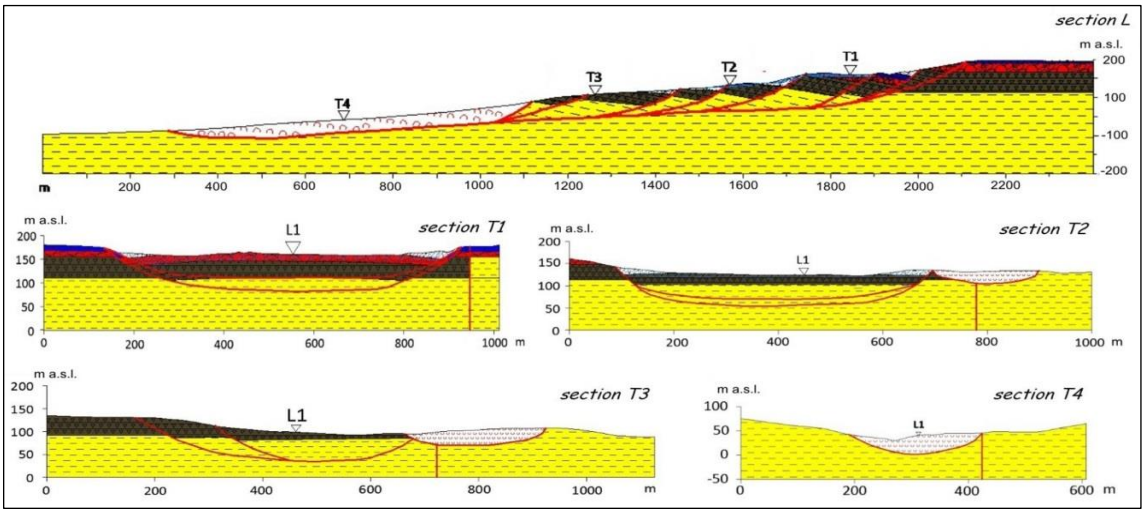

Figure 25 : Geological cross-sections constructed along the traces L, T1, T2, T3 and T4 of Figure 24.

4.3.1 Description of the numerical models

To assess the local seismic response of the Büyükçekmece landslide in terms of wave amplification pattern along the slope surface and to define possible relations with the geological setting of the slope and its topography, numerical simulations were undertaken on the longitudinal (L) and on the four transversal (T1, T2, T3 and T4) cross sections of the landslide using the 2D finite difference code FLAC 7.0 (Itasca 2011). Two additional models, namely a homogeneous slope and a homogeneous landslide (not commented here), were also created for the longitudinal cross section L in order to shed light on the

parameters controlling the spatial variations of ground-motion amplifications along the slope surface. Below is a description of the main steps of the modeling with FLAC software for the longitudinal cross-section.

A similar procedure was adopted for the other cross-sections. The parameters used for the modeling are reported in Table 2 in which the colors refer to the same colors of the soils and rocks units of Figure 25.

Ta**ble 2 :** Parameters considered for the numerical simulations (colors identify the same units of soils and rocks as in Figure 24)

Unit	Vs (m/s)	Vp (m/s)	Density (kg/m³)
Earth-flows debris	148	259	1800
Debris	156 - 183	273 – 321 in dry zones 1079 – 1306 in wet zones	1800
Calcarenites	190 – 255	334 - 445	2400
Sands and gravels	203 - 270	357 – 476 in dry zones 1600 in wet zones	1800
Clays with tuffs	226 - 373	397 – 656 in dry zones 1571 - 2000 in wet zones	2000
Silty-clays	366 - 452 in the landslide mass 600 - 1000 in the substratum	642 – 793 in the landslide mass 1052 - 1757 in the substratum	2100

4.3.2 Mesh, boundary conditions and material constitutive model

The landslide area was divided into quadrilateral zones allowing an accurate representation of wave transmission through the model up to 10 Hz (Kuhlemeyer and Lysmer, 1973). Based on the materials properties (in particular the minimum shear-wave velocity Vs) and the frequency content of the input motions (in particular the maximum frequencies), in the main zone of interest (ie. namely inside the landslide mass), the element size is approximately 2-3m by 2-3m resulting in a total number of nodes equal to 80 750 nodes. Absorbing quiet boundaries (Kuhlemeyer and Lysmer, 1973) and free field boundaries (Cundall et al., 1980) were applied along the base of the model and the lateral boundaries respectively to prevent the reflection of outward propagating waves back into the model. A linear visco-elastic model was applied to all layers. Energy dissipation in the soil was solved using a Rayleigh damping function, a commonly used method to provide damping that is approximately frequency-independent over a restricted range of frequencies (Itasca, 2011). We used a critical damping ratio (also known as the fraction of critical damping) equal to 2% in the zones of interest of the model and 0.5% elsewhere (i.e., in the substratum).

4.3.3 Seismic input

4.3.3.1 Synthetic seismogram

A first order Ricker wavelet (ie. Gabor function, Semblat & Pecker, 2009) containing main frequencies in the range 0.1 to 10 Hz was applied in the form of a vertically upward propagating SV stress wave (Figure 26 et Figure 27). Signal duration is 10 s but only the first 0.15 s are characterized by non-null values. To prevent numerical errors during the dynamic calculation, this input record was checked for baseline drift: indeed, we checked that no continuing residual velocity or displacement existed after the motion had finished. This input was selected to validate the model: in particular, the propagation of the seismic signal inside and along the surface of the model was analyzed to check that no spurious reflections come back into the model from the quiet boundaries, and the numerical transfer and amplification functions were assessed and compared with the empirical ones.

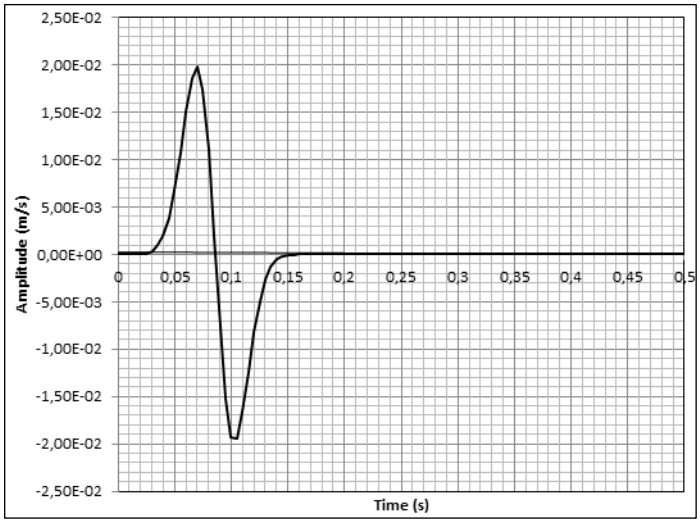

Figure 26: Zoom on the Ricker wavelet signal considered as input for the modeling.

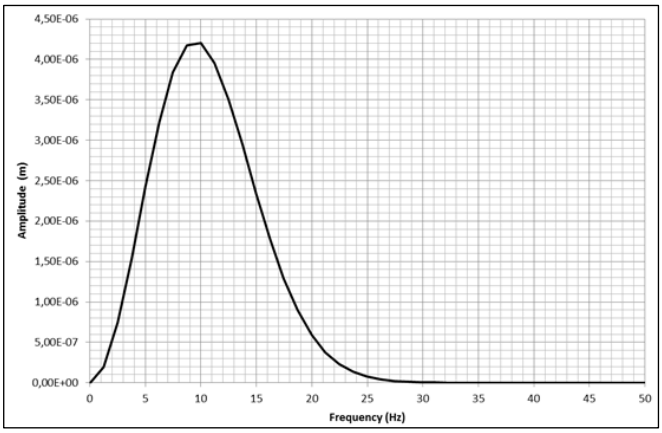

Figure 27: FFT amplitude of the Ricker wavelet (see Figure 26) used for the modeling.

4.3.3.2 Recorded seismograms

3 among the 45 recorded earthquakes at TEPT reference station were selected to perform numerical simulations (earthquakes EQ22, EQ33 and EQ37 of Table 1 and Figure 19, and figures from 28 to 30). These signals were applied in the form of a vertically upward propagating SV stress waves (Figure 27). To prevent numerical errors during the dynamic calculation, these input records were also checked for baseline drift: indeed, we checked that no continuing residual velocity or displacement existed after the motions had finished.

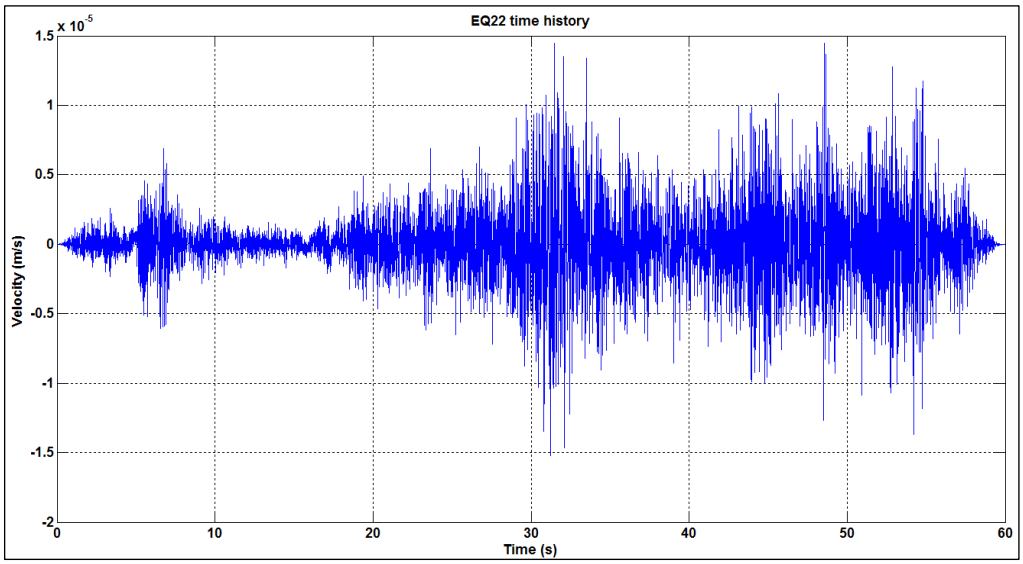

Figure 28: Velocity time history of EQ22 recorded at TEPT station and considered for the numerical modeling.

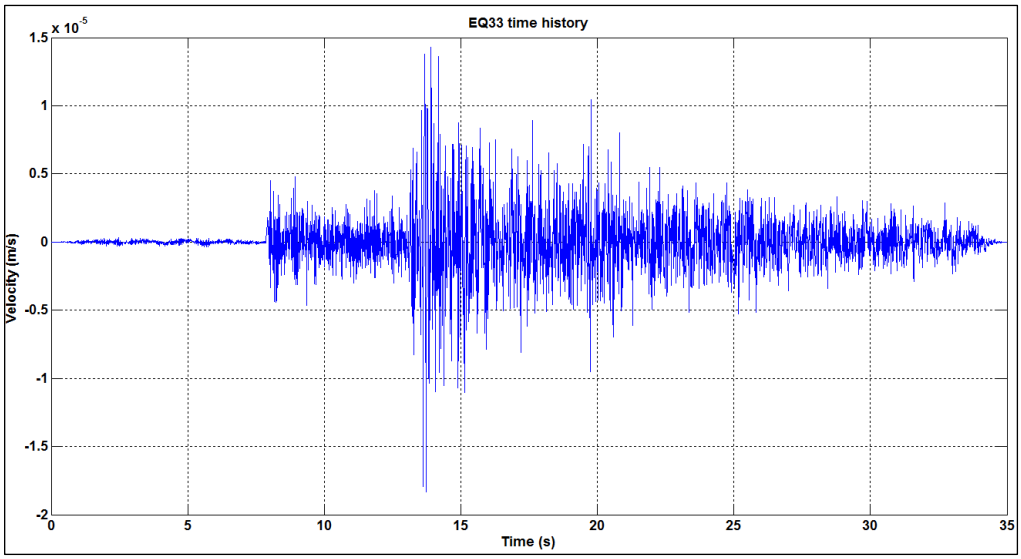

Figure 29: Velocity time history of EQ33 recorded at TEPT station and considered for the numerical modeling.

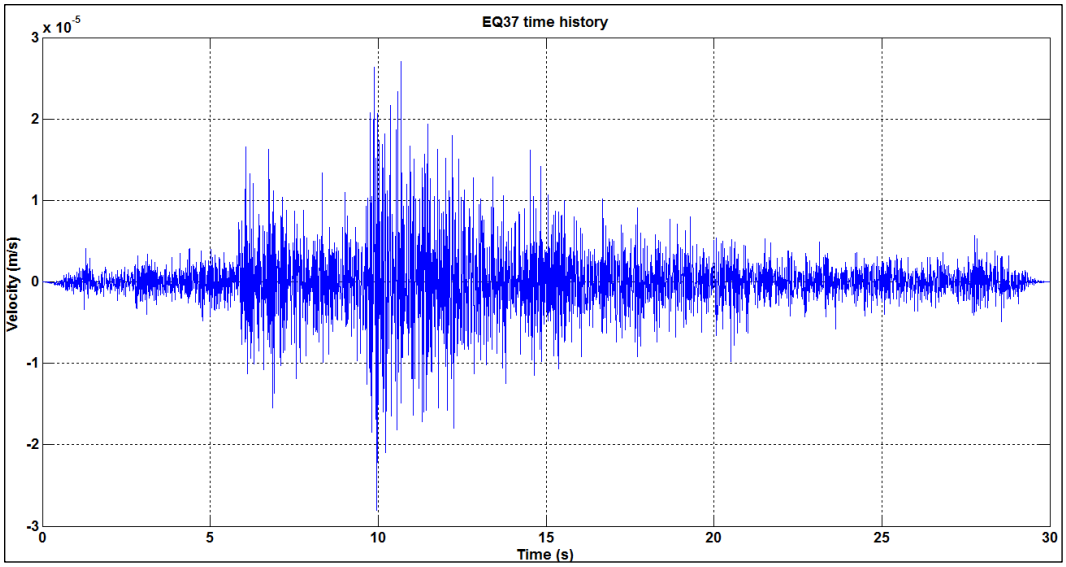

Figure 30: Velocity time history of EQ37 recorded at TEPT station and considered for the numerical modeling.

These signals were band-pass filtered between 0.1-15 Hz to take into account numerical limitations due to the mesh properties of the model. In Figs.31-33 the resulting FFT amplitudes are also reported.

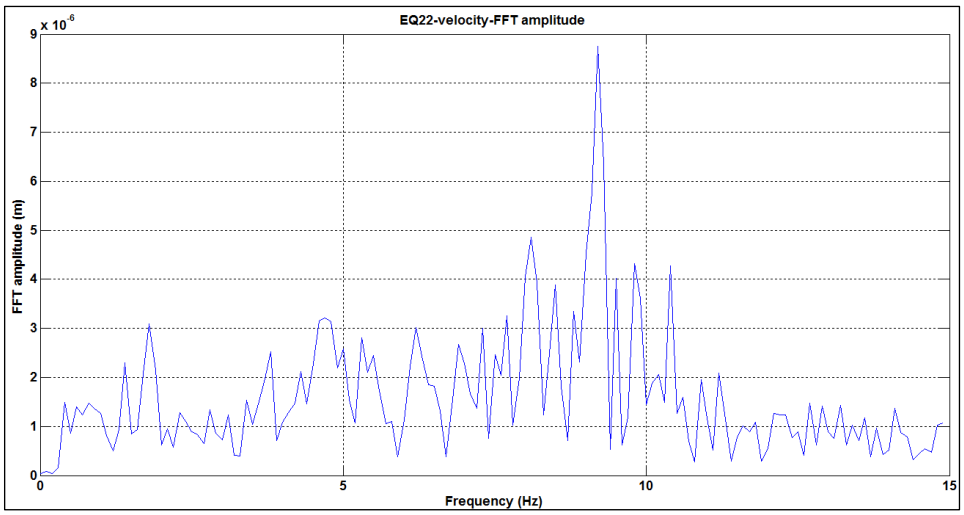

Figure 31: Velocity FFT amplitude of EQ22 recorded at TEPT station and considered for the numerical modeling.

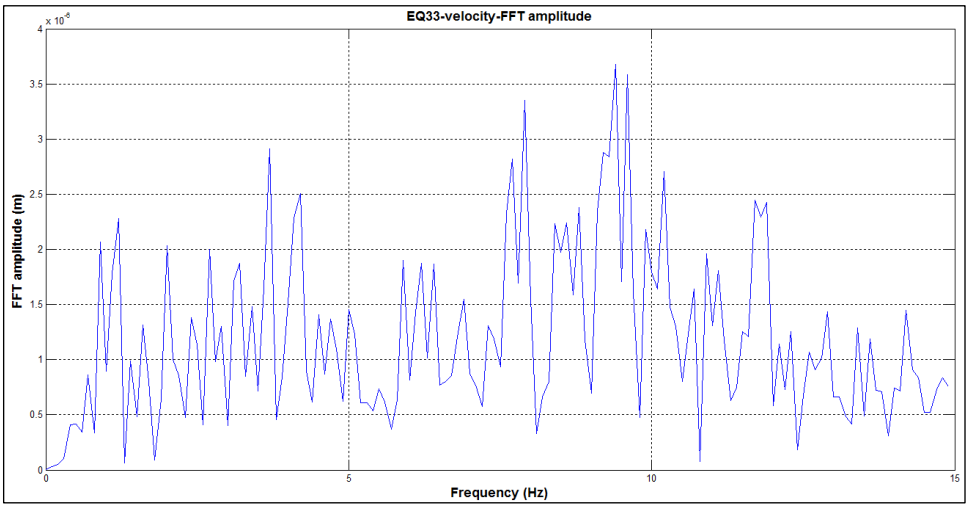

Figure 32: Velocity FFT amplitude of EQ33 recorded at TEPT station and considered for the numerical modeling.

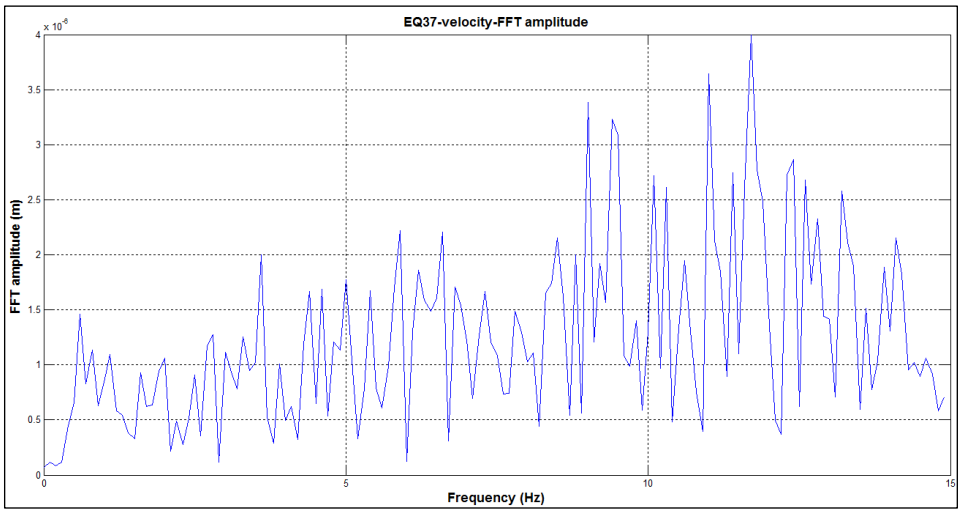

Figure 33: Velocity FFT amplitude of EQ37 recorded at TEPT station and considered for the numerical modeling.

4.4 Results on the numerical modeling of the seismic local response

For all the modelled cross-sections, Figs. 34-35 and Figs. 37-40 show (from the top to the bottom) the propagation pattern of displacements along the surface, the amplification function and the geological setting of the models. The plots showing the propagation of seismic waves using as input the Ricker wavelet put in evidence that no spurious reflections of waves come back from the boundaries of the models.

Amplification functions are obtained calculating the ratio between the FFT amplitude of the velocities computed along the surface of the models and the FFT amplitude of the velocity computed at a reference station selected in a point of the model which represents the outcropping bedrock. Each section was also modelled considering a homogeneous material, i.e. reproducing only its topographic shape. For instance, Fig. 34 illustrates the results for the longitudinal cross-section L. This plot shows that topographic effects cannot be responsible for any amplification. A comparison between Fig. 34 and Figs. 35, 37-40 shows that seismic amplification at the landslide site is very complex and strongly controlled by the geological setting of the slope. For the longitudinal cross-section L, hardly any amplification is observed, outside from the landslide area while strong amplifications (about 3) are observed in the landslide mass at frequencies between 2 and 4 Hz. To further shed light on the parameters controlling such an amplification pattern, we also computed ground-motion amplifications in 1D soil columns representing only the 1D geological setting of the landslide at given locations along the cross-section. The results (not shown in this report because only preliminary) show that the amplifications computed in the 2D cross-section are mainly controlled by the impedance contrast between the landslide mass debris and the local substratum (i.e. seismic bedrock).

On the edges of tilted landslide blocks, seismic amplification effects result at higher-frequencies respect to the remnant landslide mass. Fig. 36 shows the comparison between the empirical amplification function computed at SU station considering TEPT as a reference and the modelled amplification computed at the same surface location along the longitudinal section L. The maximum values of the amplification functions obtained for the longitudinal section and the transversal ones are close to 3 and 2.5 respectively. The numerical modelling outputs agree quite well with empirical data in the frequency range 2-8Hz while at lower frequencies an important misfit remains. To better explain such differences, more specific analyses should be conducted to detect if such an effect can be related to the depth of the seismic input in the numerical model, or to a decreasing efficiency of the quiet boundaries of the numerical domain at low frequencies.

A good agreement also exists between the natural SSR function SU/TEPT and the numerical one (Fig. 36) even if a noticeable shift of the function can be observed starting from the second peak of the computed function. Again, more detailed simulations will help in the future to better understand the reasons of such a discrepancy.

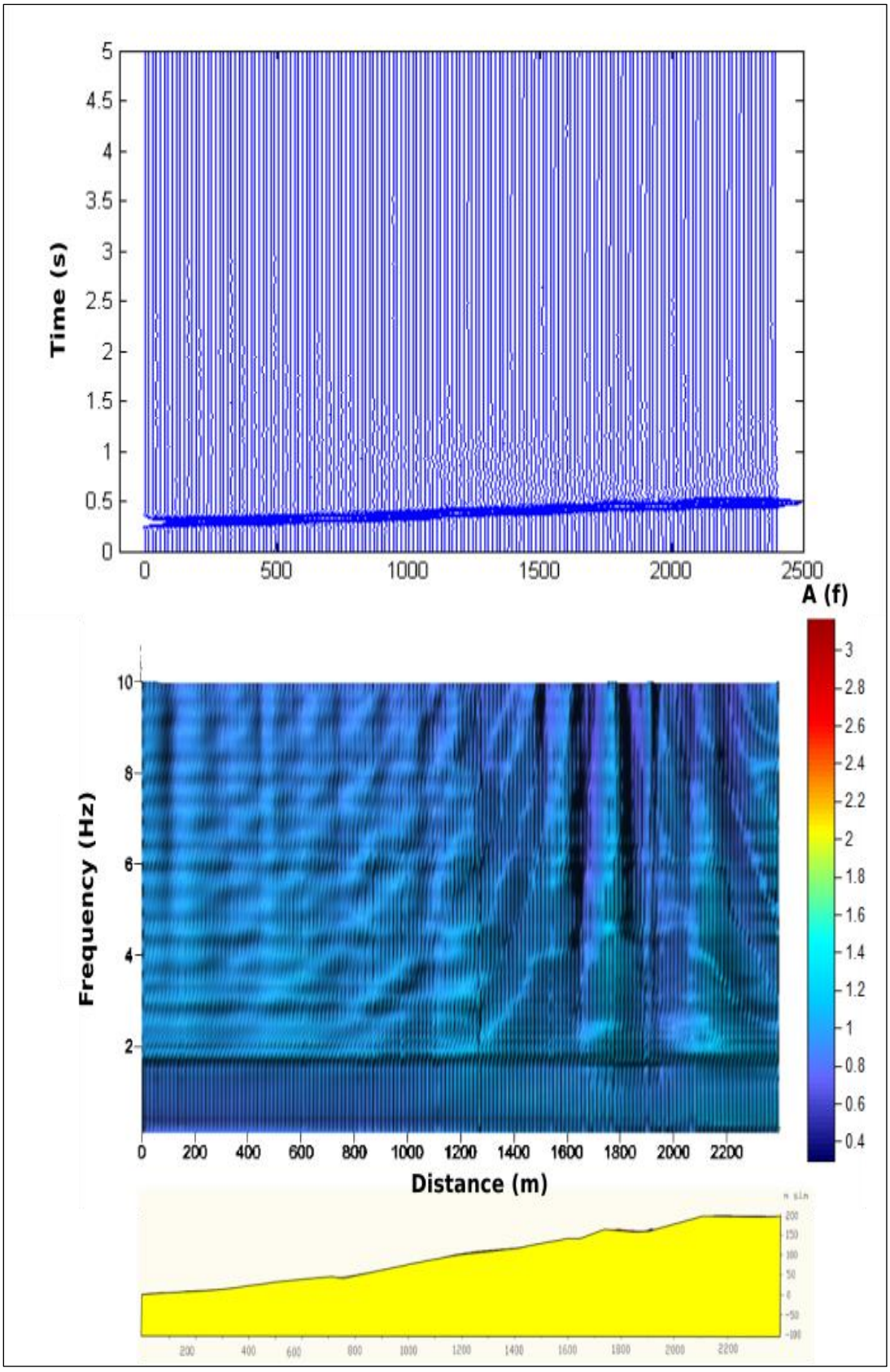

Figure 34 : From the top to the bottom: propagation along the cross-section L (see Figs 24-25) as revealed by displacements histories versus time, amplification function and model considered (homogeneous).

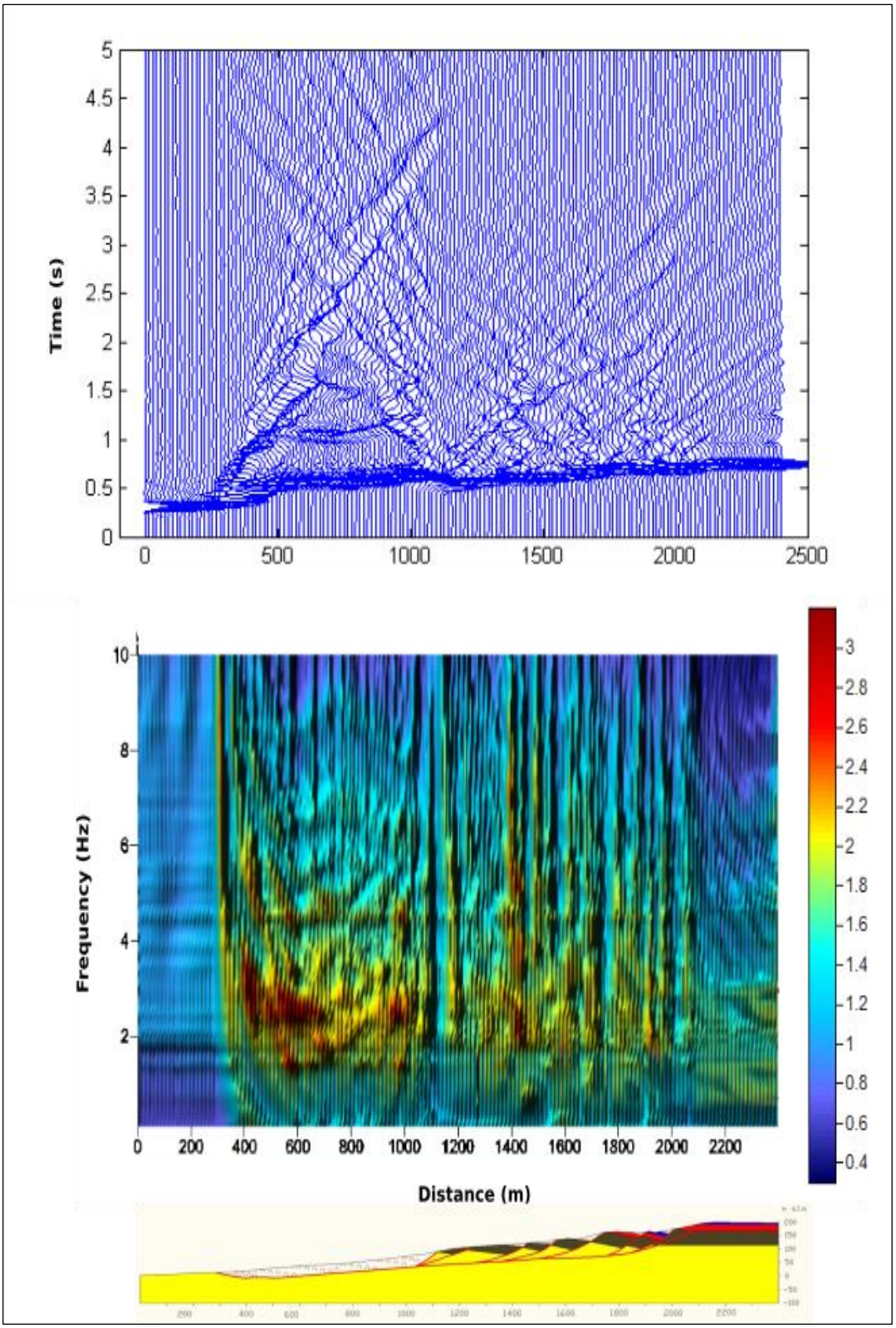

Figure 35: From the top to the bottom: propagation along the cross-section L (see figs 24-25) as revealed by displacements histories versus time, amplification function and model considered (heterogeneous filling within the landslide).

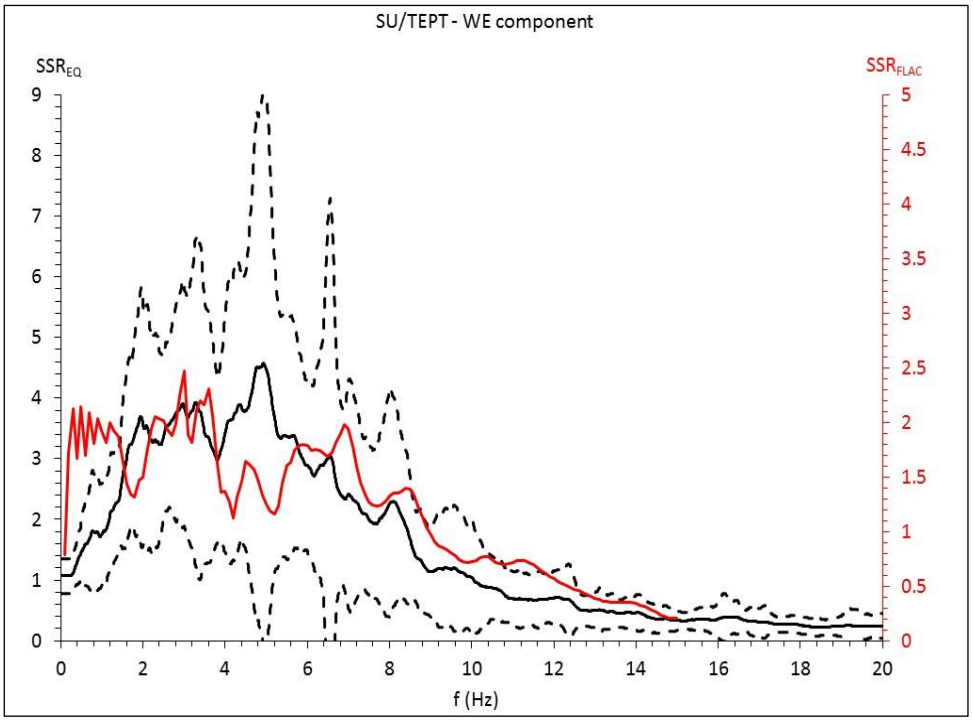

Figure 36 : Cross-section L: SSR of the earthquakes selected for the numerical modelling (see Fig. 19 for the epicentral locations) and recorded at TEPT and SU stations compared with the numerically derived SSR function obtained by FLAC (red line). The standard deviation (dashed lines) for the average SSR from the 45 recorded earthquakes is also shown.

From these results, we can conclude the impedance contrasts between the landslide mass and the substratum can be regarded as responsible for a very complex and broadband seismic response at the Büyükçekmece landslide site and that the topographic effects are hardly responsible for any amplification. This latter result could be expected because the slope angle of the slope hosting the landslide is very low (only 4°) resulting into low amplifications if any. All the simulations performed up to now consider a seismic input applied at the bottom of the model in the form of an in-plane SV stress wave with a vertical incidence. Nevertheless, the proximity and the dimension of the NAFZ should be taken into account in future simulations considering also non-vertical seismic inputs. Moreover, further analyses should be devoted to the study of the amplification effects under nonlinear conditions, i.e. accounting for stiffness decay and damping increase of the superficial materials. In this regard, it is worth stressing that no suitable dynamic properties are available for the materials involved in landslide mass since the ones deduced from the lab-tests performed in the framework of the MARSite project on the materials sampled during the borehole drilling were too much remolded.

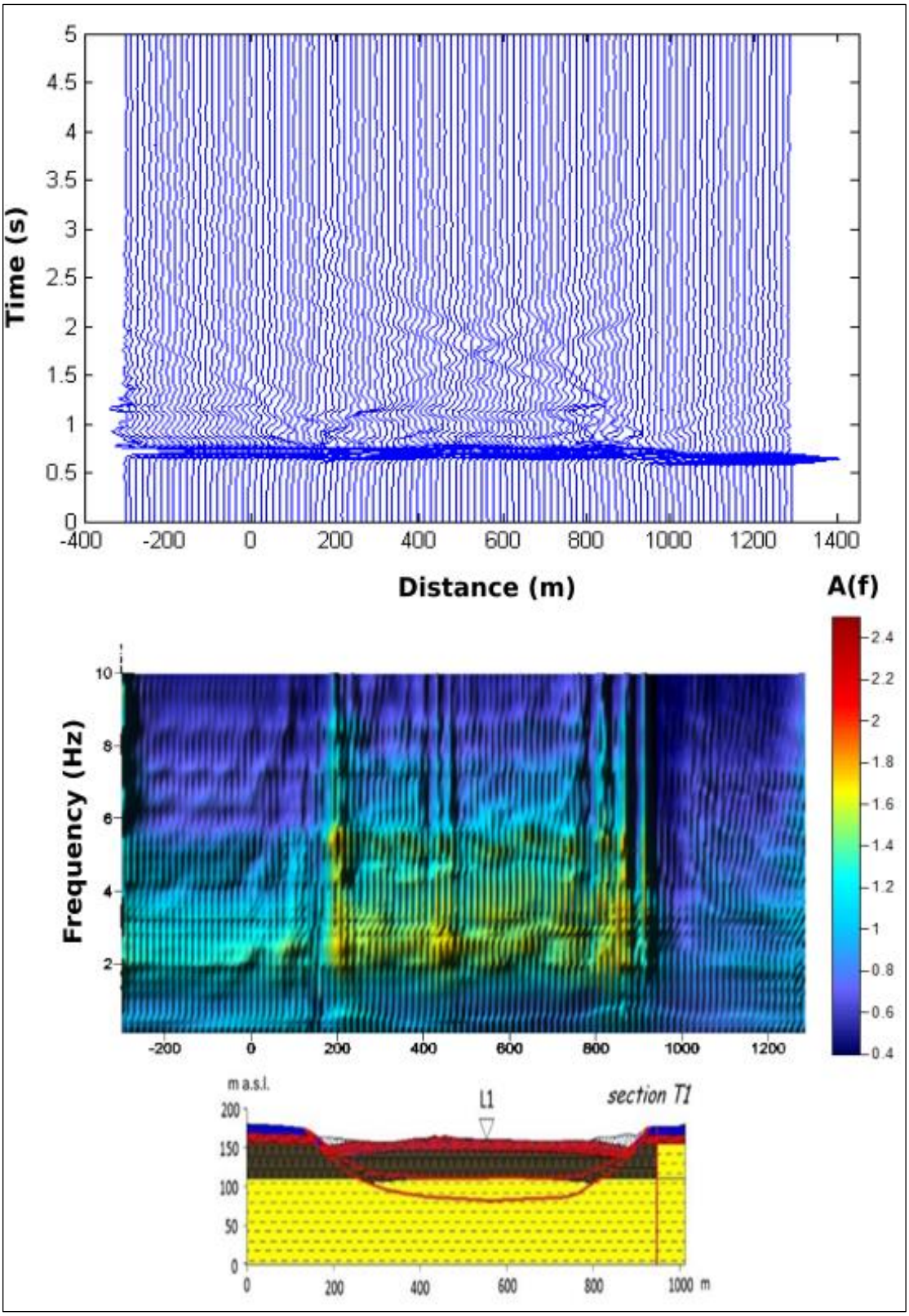

Figure 37 : From the top to the bottom: propagation along the cross-section T1 (see Figs 24-25) as revealed by displacements histories versus time, amplification function and the geological-cross section considered for the modelling (see Fig.24 for legend)

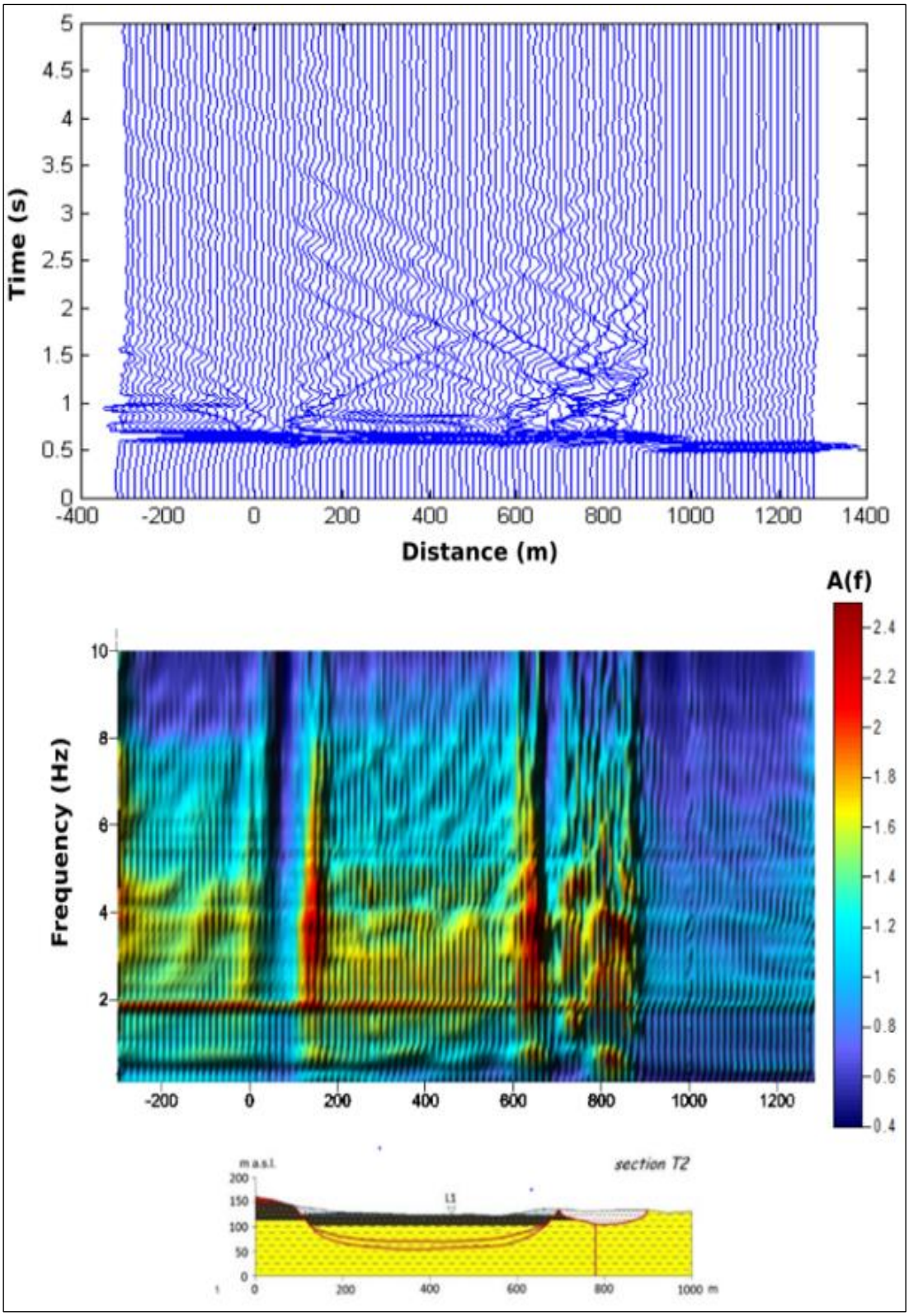

Figure 38 : From the top to the bottom: propagation along the cross-section T2 (see Figs 24-25) as revealed by displacements histories versus time, amplification function and the geological-cross section considered for the modelling (see Fig.24 for legend)

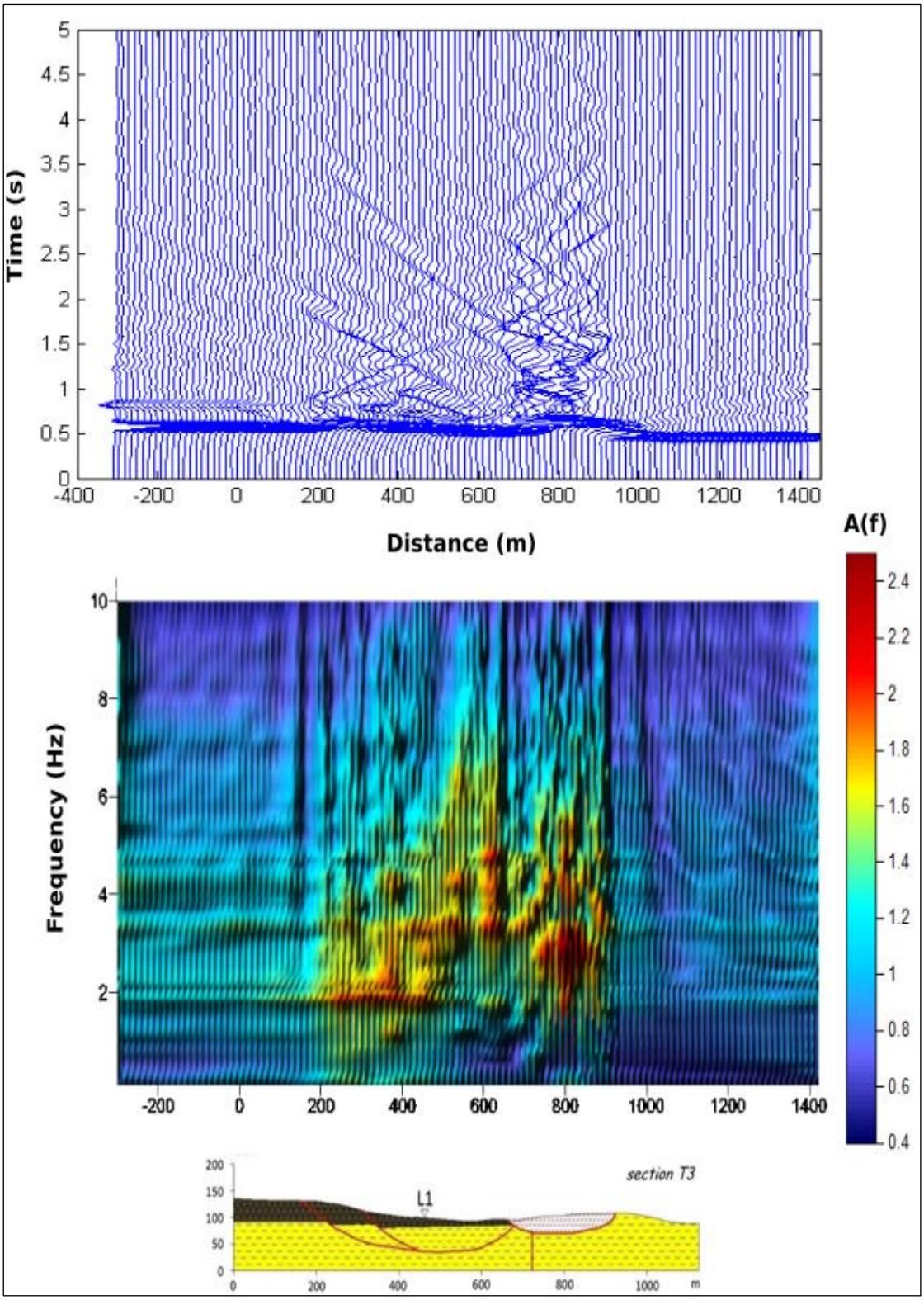

Figure 39 : From the top to the bottom: propagation along the cross-section T2 (see Figs 24-25) as revealed by displacements histories versus time, amplification function and the geological-cross section considered for the modelling (see Fig.24 for legend)

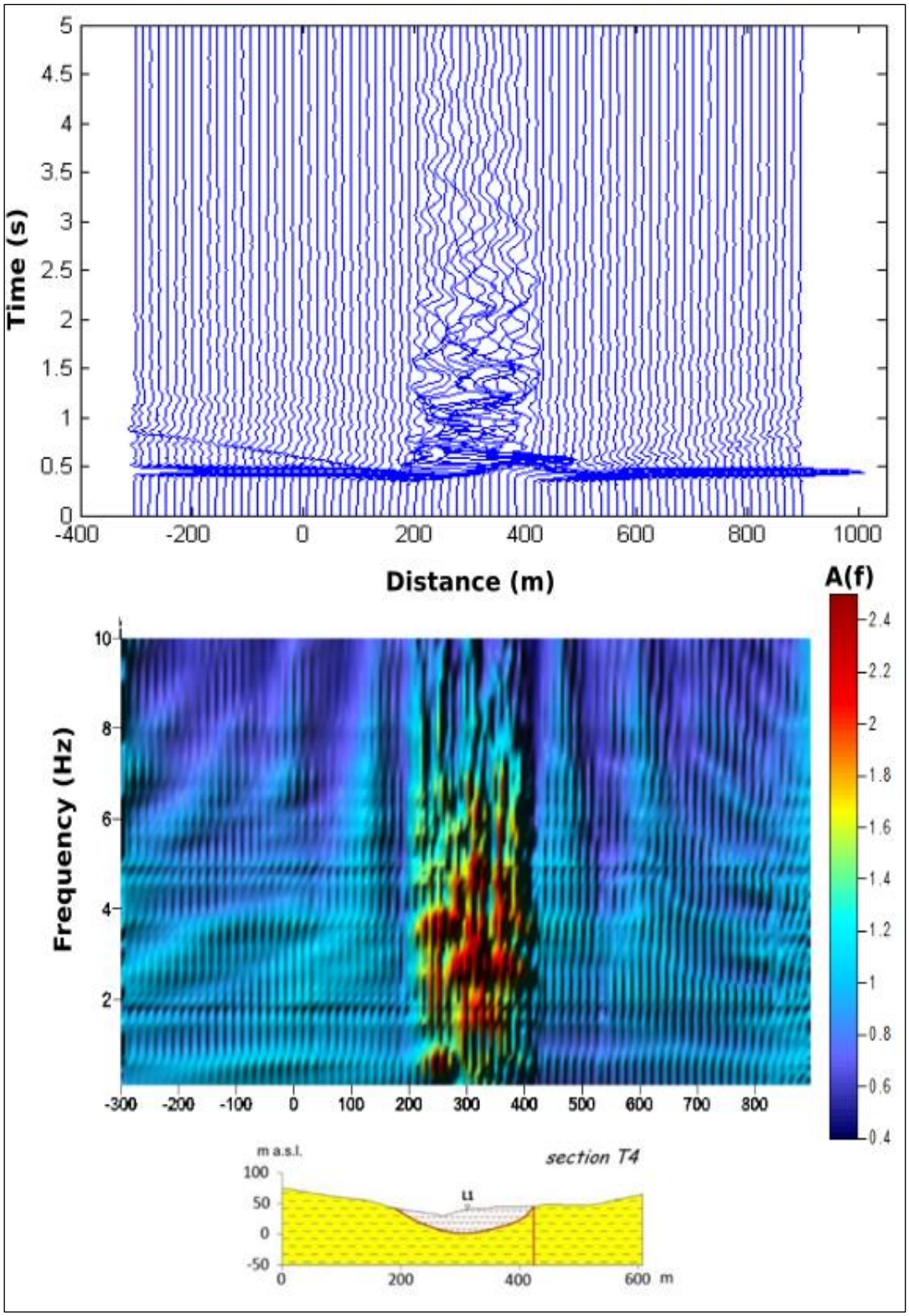

Figure 40 : From the top to the bottom: propagation along the cross-section T4 (see Figs 24-25) as revealed by displacements histories versus time, amplification function and the geological-cross section considered for the modelling (see Fig.24 for legend)

4.5 Numerical modelling of earthquake-induced landslide mass mobility (LMM)

The LMM analysis of the Büyükçekmece landslide under dynamic conditions was performed by applying several inputs to the FLAC numerical model (longitudinal L cross-section) and computing the resulting displacement fields within the landslide mass. To this aim, a customized script was written for managing the computed displacements inside and outside the landslide mass and calculating the movement to quantify the effective horizontal displacement (x-disp) with respect to the substratum. Moreover, according to Lenti & Martino (2013), the x-disp values were defined considering different percentages of the landslide mass with the largest displacements (i.e., 5%, 15%, 30%, 50% and 100%). The seismic inputs for the numerical models were derived by selecting 15 accelerometric records of the European database together with records from the K-NET and COSMOS databases because they include a wide typology of seismic signals. These inputs are characterized by the Arias intensity (AI) on the order of 0.01 m/s and different values of the characteristic period, T_m, ranging from 0.3 to 16.5 s. Depending on landslide dimensions, the computed T_s is equal to 0.63 s while T_l is equal to 0.36 s. As a consequence, the values of the T_s/T_m ratio are in the range of 0.04 – 3.31 while the values of the T_l/T_m ratio are in the range of 0.02 – 1.9.

In the case of the Büyükçekmece landslide, the T_l value was computed with respect to the length of a single landslide block (i.e. about 130 m) within the landslide mass, which is divided into several sub-masses by secondary scarps and sliding surfaces corresponding to the several orders of surveyed counter-slope terraces. This choice is justified since the peak of the x-disp vs. T_l/T_m curve well corresponds to the theoretical value of 0.5, according to the single-block length and not for the total landslide mass length (i.e. 1830 m).

To perform the LMM analysis, the time histories of the selected inputs were scaled to have AI values of 0.001 and 1 m/s without modifying the T_m; in this way, 36 inputs where available for this landslide, representative of three energy levels in a wide range of T_m values. Moreover, to perform the dynamic modelling, an equivalent signal was associated with each selected input according to the LEMA_DES (Levelled-Energy Multifrequential Analysis for deriving Dynamic Equivalent Signals) approach by Lenti & Martino (2010). The LEMA_DES procedure generates a sequence of functions and signals that 1) provide with a selection of characteristic frequencies from a smoothed Fourier spectrum of a reference accelerogram; 2) achieve a null integral over the entire duration of the final signal and a spectral density that is negligible at frequencies lower than the minimum characteristic one, and 3) produce a resulting multi-frequential dynamic equivalent signal that is energy-equivalent to the reference signal, best-fitted in terms of PGA via an iterative procedure performed on the number of equivalent cycles and whose time duration is significantly shorter than that of the reference signal. The use of this approach in dynamic numerical modelling guarantees (Lenti and Martino, 2010): 1) the frequency content of the derived signals is defined within a representative/admissible range; 2) the upper-threshold frequency is avoided in the modelling; 3) the energy gap between the real and simulated seismic actions is narrowed; 4) the maximum intensity of the adopted action is controlled; and 5) the computational time is reduced (especially in the case of parametric analyses, where a high number of iterations is required), as the equivalent input is typically shortened with respect to the reference one.

Following the CPB approach (Figure 41), the obtained results were plotted on graphs showing the computed x-disp for each applied input, corresponding to the characteristic ratios T_s/T_m and T_l/T_m. These distributions allow discussing the roles of both the 1D resonance and the 2D input-slope interaction in the calculated displacements, as they are related to the T_s/T_m and T_l/T_m, respectively.

As it resulted from the numerical modelling, in the case of the Büyükçekmece landslide, at the lowest AI values the maximum earthquake-induced displacements result

for T_m close to the landslide-block mass resonance period (i.e., to a T_s/T_m ratio almost equal to 1, Figure 41). This result is in agreement with the $HVSR_s$ obtained from noise and earthquake records, the SSR_s obtained from earthquakes and the 2D numerically derived ones that reveal a significant seismic amplification related to the resonance of the landslide mass.

On the other hand, for increasing AI (up to 1 m/s) the maximum computed displacements result for long period signals, i.e., whose T_m is almost equal to $2T_I$. Moreover, the higher the AI is, the more relevant the role of 2D interactions between landslide mass and seismic waves is. This result indicates that in the case of strong motion, the Büyükçekmece landslide could exhibit larger displacements for long period earthquakes, i.e., with T_m significantly lower than the landslide T_s. In the graphs of Figure 41, the displacement values from the traditional sliding block methods correspond to $T_s/T_m=T_I/T_m=0$, as they were obtained according to literature correlations (Lenti and Martino, 2013 and references therein) existing among the critical pseudostatic coefficient of the landslide, the PGA and/or the AI value of the input, i.e., independent of its spectral content. These differences are justified because the traditional approaches cannot consider the increasing displacements at low T_I/T_m ratios, i.e., related to seismic wave propagation within the landslide mass with a predominant half-period very close to the length of the landslide mass. It is noticeable that in the case of Büyükçekmece landslide, Newmark displacements (also considering the flexible block approaches) are negligible for all the considered AI values of the inputs as they result lower than 1 mm.

A specific numerical modelling was also carried out by considering the seismic input obtained by the WP5, i.e. for a return period of 475 yrs with a AI value in the order of 0.1 m/s and a T_m of 0.89; the obtained modelled x-disp are in very good agreement with the aforementioned theoretical curve of LMM since they result in the same order of magnitude if computed for the lowest percentage of landslide mass while they are coincident if the whole landslide mass is considered. The here obtained LMM results are also in agreement with the displacements monitored during the MARsite project; indeed, the lack of correlation between the displacement rates and the earthquakes recorded can be related to the very low AI values ($<10^{-3}$ m/s) of the recorded seismic events.

To account for effects due to the water pressure distribution within the Büyükçekmece landslide mass the data monitored during the MARsite project were considered. To this aim, the reconstruction of the hydrogeological setting was based on engineering-geological criteria and observations of World Imagery pictures published by ESRI. It was hypothesized that the main direction of the groundwater flow is almost SE-NW, and that a part of the drainage of the plateau, partly feeds the earth-flow on the left flank of the landslide, and partly infiltrates in the landslide mass, just along the main shear zone. Moreover, taking into account the back-tilted blocks that constitute different orders of landslide terraces, and examining the hydraulic connections among them, it was proposed a flow system regulated by overflow thresholds. In this regard, if the groundwater flow exceeds the thresholds the drainage occurs in the whole rototranslational landslide mass. Considering the reconstructed groundwater table, a specific stress-strain numerical modeling was performed using FLAC under dynamic configuration considering the same inputs used for analyzing the dry conditions. The obtained results demonstrate that, in terms of computed x-disp values, no relevant effects can be attributed to the most severe water pore pressure scenario admissible for the landslide mass with respect to dry conditions.

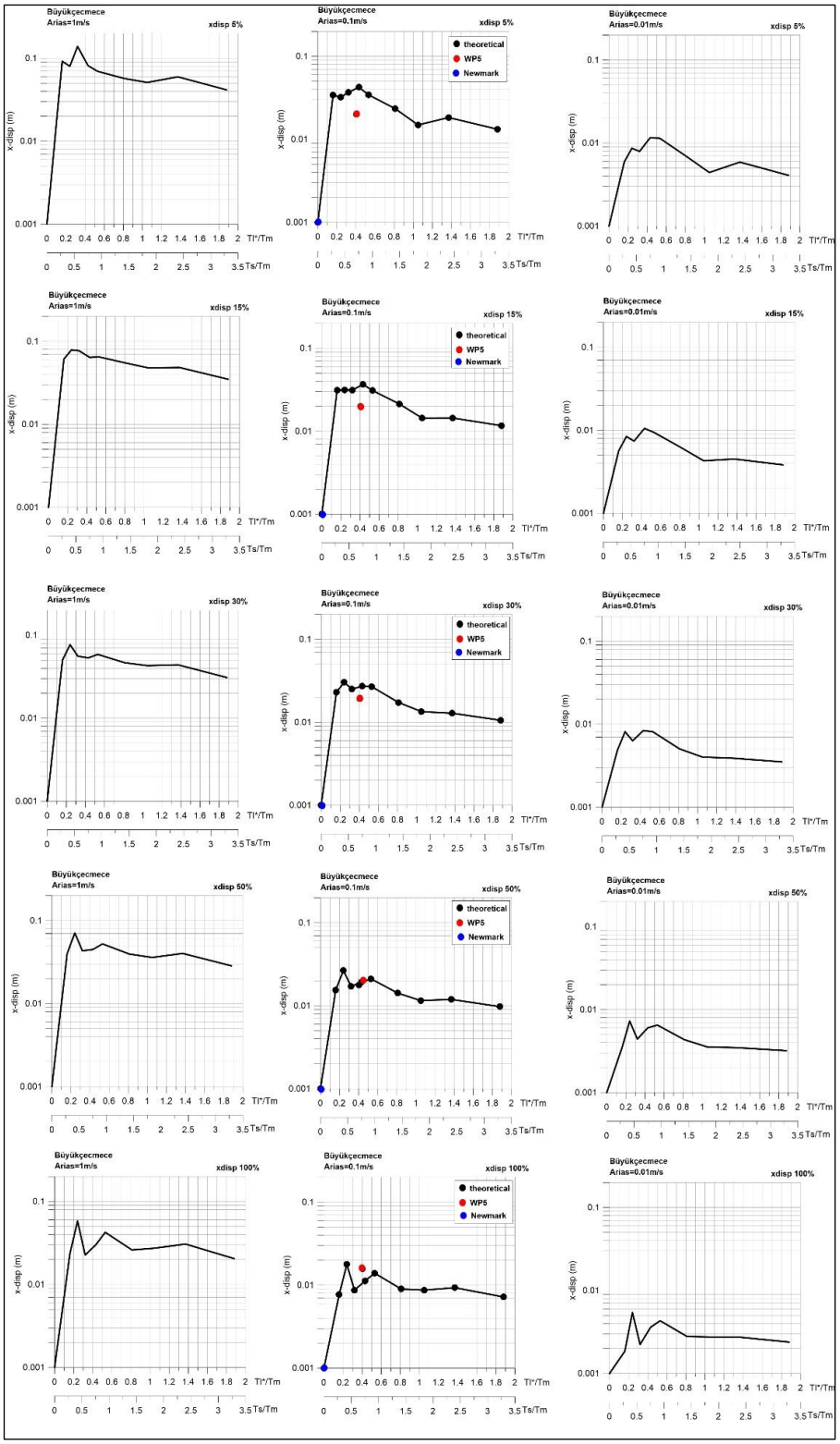

Figure 41 : Results of the LMM numerical modelling performed according to the CPB approach. The rows report the output for different percentages of the landslide mass while the columns refer to different AI values.

5 Discussion and Conclusions

This report has presented the results of the task 2b for the on-shore area, the Cekmece-Avcilar peninsula, in detail for the selected representative unstable slope of this area, the Büyükçekmece landslide.

This landslide is classified as composite mechanism. It includes rototranslational parts, several secondary scarps, several landslide terraces (these last ones are characterized by an evident counter slope and some of them are responsible for the presence of water pools), evidences of two earth flows; the first one located along the right side of the landslide mass and the second one at its toe (these earth flows are clearly visible in the field due to the presence of detachment and transportation zones). Several evidences of damage to roads, buildings, walls, and infrastructures were also collected and considered for mapping the landslide mass.

On this landslide INERIS installed a local multi-parameter observational system to collect time series for a better understanding of landslide mechanism. Based on the first time-series, the landslide moves continuously toward W; a double-net groundwater flow is revealed by the piezometer monitoring and preliminary co-relations between pore water pressures and rainfalls are evident in a seasonal and monthly time interval respectively. The 81 earthquakes recorded by the surface and deep INERIS seismic 3C seismic stations demonstrate any particular amplification due to the landslide mass (recall that the two stations are located at the same point but at a different depth). The surface station has PGA values major than deep station, so there is a local amplification along the vertical profile due to the depth. It is worth to notice that the deep station is locate above the probable sliding surface, so the vertical stratigraphic profile is pretty the same for both stations. The absence of other stations in different points of the landslide area does not permit to study any kind of amplification due to the landslide mass.

From a technical point of view, the multi-parameter system was subject to different breakdowns, so we have some data gaps for seismic activity and rainfall data. In addition, there were the malfunction of the moisture sensor and the cut of the cable of the deep station. The results of the geophysical measurements show that the Buyukcekmece landslide includes several failure surfaces, whose depths change between 10–60 m, probably one of these is responsible for the cable cut. The measurements recorded by the moisture sensor are inconsistent in comparison with other data from the weather station. This problem may come from: a soil saturated with water or a technical problem directly related to the sensor.

The performed noise measurements by IU pointed out anthropic vibrations (focused at about 1.5Hz) that could alter data interpretation as they interfere with the natural resonance. Neglecting the anthropic peaks in the HVSR analysis, since they do not show polarization along a given direction, the obtained curves indicate that the landslide area is characterised by higher resonance frequencies (generally >2Hz) than the sites located outside from the landslide.

Based on several performed geophysical investigations by IU, landslide geometry and dynamic soil properties were derived and used by IFSTTAR-La Sapienza for reconstructing a detailed engineering-geological model and for 2D numerical simulation in viscoelastic condition. As it resulted from these analyses, the 2D amplification function derived by stress-strain modelling is strongly influenced by the local geological setting and shows relevant amplifications in the slope at frequencies between 2 and 4 Hz, that can be related to the impedance contrast between the landslide mass debris and the local substratum (i.e. seismic bedrock).

5.1 Future perspectives

Because of insufficient time and staff the following activities remained incomplete. Some of them will be completed within the next couple of months.

5.1.1 Dynamic mapping

At the beginning of the MARsite project in order to obtain a fully automatic hazard map creation, the ArcGIS ModelBuilder application was used as it fits the automation problematic perfectly. It is based on two kinds of data:

- Invariable Data: the geology and the topology do not change in time and are invariables parameters in the model and are therefore stored in the geodatabase (they can however be updated manually in the active geodatabase if needed).
- Dynamical Data: the seismic information (shaking maps, ground motion parameters, etc) are variable parameters in time. This data comes from an external server where the data can be updated externally. The path to this server is given in the model. This enables the model to automatically take in account the near real time updates of the event. It is very important that the nature, format and coordinates of the external information correspond to those expected as input for the model.

As to dynamic data:

- Shaking maps: is a shapefile of polygons. Each polygon delimits an area with the same Peak Ground Acceleration. The attribute table includes the value of acceleration (mg). This file was artificially created in the aim of constructing the automatic GIS structure. The file should be provided by WP9. The model will then have to be adapted to its format.
- Earthquake characteristics: is a table file. It gives the earthquake characteristics. The table contains the X position, the Y position, the depth (the hypocenter coordinates) and the magnitude. This file was artificially constructed to integrate parameters needed for the calculation of the co-seismic displacement.

Therefore, the ongoing steps are to update the dynamic data (shaking maps and earthquake characteristics) with seismic activity recorded by Ineris local network and results of the WP9 (if they are accessible).

In addition, rainfall integration in the tool will carry out: no consequent work has been done for the moment in the integration of rainfall in the GIS. The influence of rain on landslides is actually due to the water table level which reduces the soil strength (except earth flows). For the moment the water table level is given and depends of the geology unit. It is planned to link that water table level to the real time quantity of rain obtained by Ineris weather station. Our rainfall data are congruent with the data of the Florya meteorological station, which is close to the Büyükçekmece landslide.

5.1.2 Local landslide early warning system

In complement to the time series visualization through e-cenaris, the implementation of an early warning tool has been designed, where the alarm may be transferred automatically to different authorities and partners with personalized notification message was also carried out.

Recall that the Cekmece-Avcilar peninsula is characterized by landslides, showing high susceptibility to both heavy rainfall and earthquakes. Therefore, an efficient early warning system has to take into account these two triggering factors.

Concerning earthquake early warning (EEW), two approaches are possible: regional warning and on-site warning. We focused on the second, based on individual sensors installed at the Büyükçekmece landslide. Generally, for on-site warning the beginning of the ground motion (mainly P waves) recorded at a site is used to predict the ensuring ground motion (S waves and surface waves) at the same site. We are working on the exceedance of specific threshold time-domain amplitude of PGA, of relationships

both between τc and Mw, and between Pd and PGV for the Marmara Region proposed by Alcik et al (2011). But the problem in our case is that we need to accumulate more data to be able to determine the best threshold values of PGA, PGV, etc. A very efficient threshold has to be verified by more data.

Real-time rainfall data compared with rainfall thresholds can be incorporated into a landslide warning system. Actually, we are working on the possibility of proposing various alarms based on real-time rainfall and pore pressure data for the Büyükçekmece landslide:

- the exceedance of "x" total cumulative rainfall over 2 days, in this case the monitoring will pass in a vigilance mode and it will be double during 48 hours;
- the exceedance of "x" bars of pore pressures, in this case the monitoring will pass in a vigilance mode and it will be double during 48 hours;
- the exceedance of "x" bars of pore pressures, of a "x" PGA, in this case the monitoring will pass in a vigilance mode and it will be double during 48 hours;
- the exceedance of "x" total cumulative rainfall over 2 days and of "x" mm of cumulative GPS displacement , etc…

The definition of all these values is ongoing.

5.2 Dissemination in the framework of MARsite project

Bigarré P., Coccia, Theoleyre F., Ergintav S., Ozel O., Yalcinkaya E., Özalabey S., Lenti L., Martino S., Gasperini L., Gamba P., Zucca F., Meisina C., Moro M., Ozeren S.. Earthquake induced landslide hazard: a multidisciplinary field observatory in the Marmara SUPERSITE. EGU, 27 Avril-2 Mai 2014, Vienne.

Bigarré P., Coccia, Theoleyre F., Ergintav S., Ozel O., Yalcinkaya E., Özalabey S., Lenti L., Martino S., Gasperini L., Gamba P., Zucca F.,Moro M. Earthquake induced landslide hazard field observatory in the Avcilar peninsula. EGU 12-17 April 2015, Vienne.

Bourdeau C., Lenti L., Martino S., Ozel O., Yalcinkaya E. 2015. "Local seismic response analysis in the large Büyükçekmece (Turkey) landslide area by detailed engineering-geological and numerical modeling". 6th International Conference on Earthquake Geotechnical Engineering, 1-4 November 2015, New Zealand.

Bourdeau C., Lenti L., Martino S. 2015. « Impact d'une géologie complexe sur la réponse sismique locale d'un grand glissement de terrain ». 9ème colloque national de l'Association Française du Génie Parasismique, 30/11 au 02/12/15, Marne-la-Vallée, France.

Bourdeau C., Lenti L., Martino S. 2015. « Local seismic response of a large landslide in the Marmara region". French-Japanese Symposium on Earthquakes and Triggered Hazards. 16/09 au 19/09/ 2015, BRGM, Orléans, France.

Bourdeau C., Lenti L., Martino S. 2015. "Numerical modeling of the seismic response of a large pre-existing landslide in the Marmara region". *European Geosciences Union Conference*, 13-17 April 2015, Vienna, Austria.

Coccia S., Theoleyre F., Bigarre P., Ergintav S., Ozel O., Özalaybey S. Advancements in near real time mapping of earthquake and rainfall induced landslides in the Avcilar Peninsula, Marmara Region. EGU, 27 Avril-2 Mai 2014, Vienne.

Coccia S., Bigarré P., Ergintav S., Ozel O., Yalcinkaya E., Özalabey S., Bourdeau C., Lenti L., Martino S., Zucca F., Moro M.. How a multidisciplinary work in the Marmara Supersite, related to Earthquake induced landslide hazard, was successfully carried out. Symposium Franco-Japonais sur les séismes et les risques induits, 16 - 18 Septembre 2015, Orléans (BRGM).

Coccia S., Bigarré P., Ergintav S., Ozel O., Yalcinkaya E., Özalabey S., Bourdeau C., Lenti L., Martino S., Zucca F., Moro M.. Results of the Multidisciplinary work in the Marmara Supersite, on-shore area: Beylikdüzü landslide. European Geosciences Union Conference, Vienna, Austria, 2016.

Martino S., Bigarré P., Coccia S., Bourdeau C., Lenti L., Ozel O., Yalcinkaya E. 2016. “Integrated engineering-geological and numerical approach applied to the large Büyükçekmece (Turkey) landslide for evaluating earthquake-induced effects”. 12th International Symposium on Landslides (ISL 2016). 12 - 19 June 2016, Napoli, Italy.

Yalcinkaya E., Ozel O., Bigarré P. Preliminary analysis of site effects at the stations located in the landslide-prone area in the western part of Istanbul, Turkey. EGU, 27 Avril-2 Mai 2014, Vienne.

6 References

Alcik H., Ozel O., Wu Y.M., Ozel N.M., Erdik M., 2011. An alternative approach for the Istanbul earthquake early warning system, Soil Dynamics and Earthquake Engineering, Special Issue Earthquake Early Warning, Vol. 31, Pages 181-187.

Allen RM, Kanamori H. The potential for earthquake early warningin Southern California.Science2003; 300:786–9.

Bard PY, SESAME-Team (2005) Guidelines for the implementation of the H/V spectral ratio technique on ambient vibrations: measurements, processing, and interpretations. SESAME European research project, EVG1-CT-2000-00026, deliverable D23.12. Available at: http://sesamefp5.obs.ujfgrenoble.fr.

Birgoren, G., Ozel, O., Siyahi, B. (2009). Bedrock depth mapping of the coast south of Istanbul: Comparison of analytical and experimental analyses, Turkish J. Earth Sci., 18, 315-329.

Cundall P., Hansteen E., Lacasse S., and Selnes P. B., 1980. "NESSI, Soil Structure Interaction Program for Dynamic and Static Problems", Norges Geotekniske Institute, Norway, Report 51508-9.

Dalgiç S (2004) Factors affecting the greater damage in the Avcılar area of Istanbul during the 17 August 1999 Izmit earthquake. Bull Eng Geol Env, 63:221–232.

Duman TY, Can T, Gokceoglu C, Nefeslioglu HA, Sonmez H.(2006) Application of logistic regression for landslide susceptibility zoning of Cekmece Area, Istanbul, Turkey. Environ Geol 51: 241–256. DOI 10.1007/s00254-006-0322-1.

ITASCA, 2011." FLAC 7.0: User manual", Licence number SN 213-33-760- clé 29753, IFSTTAR.

Kanamori H ,Maechling P, Hauksson E.Continuous monitoring of ground- motion parameters. Bull Seismol Soc Am 1999;89:311–6.

Konno K., Ohmachi T. (1998). Ground motion characteristics estimated from spectral ratio between horizontal and vertical components of microtremors. Bull. Seism. Soc. Am. Vol. 88, n. 1, 228-241.

Kuhlemeyer, R. L., and J. Lysmer, 1973. "Finite Element Method Accuracy forWave Propagation Problems", J. Soil Mech. & Foundations, Div. ASCE, 99(SM5), 421-427.

Lenti, L. & Martino, S., 2010. "New procedure for deriving multifrequential dynamic equivalent signals (LEMA_DES): a test-study based on Italian accelerometric records", Bulletin of Earthquake Engineering, 8, 813-846.

Lenti, L. & Martino, S., 2012. "The interaction of seismic waves with step-like slopes and its influence on landslide movements", Engineering Geology, 126, 19-36.

Lenti, L. & Martino, S., 2013." A parametric numerical study of the interaction between seismic waves and landslides for the evaluation of the susceptibility to seismically induced displacements", Bull. Seism. Soc. Am., 103, 33-56.

Özel O., Cranswick E., Meremonte M., Erdik M., Safak E. (2002). Site Effects in Avcilar, West of Istanbul, Turkey, from Strong- and Weak-Motion Data. Bulletin of the Seismological Society of America, 92(1): 499–508.

Semblat J.F. & Pecker A., 2009. "Waves and vibration in soils: Earthquakes, Traffic, Shocks, Construction works", IUSS Press, Pavia (Italy), p. 499, ISBN: 978-88-6198-030-3.

Sørensen, M. B., I. Oprsal, S. Bonnefoy-Claudet, K. Atakan, P. M. Mai, N. Pulido, and C. Yalciner (2006). Local site effects in Atakoy, Istanbul, Turkey, due to a future large earthquake in the Marmara Sea,Geophys. J. Int.167,1413–1424, doi 10.1111/j.1365-246X.2006.03204.x.

Tezcan, S. S., E. Kaya, I. E. Bal, and Z. Ozdemir (2002). Seismic amplification at Avcilar, Istanbul, Eng. Struct.24,661–667

Varnes DJ (1978) Slope movement types and processes. In: Schuster R.L. & Krizek R.J. (Eds.), Special Report 176 Landslides: Analysis and Control. Transportation Research Board, National Research Council, Washington D.C., 11-33.
Wu YM, Kanamori H, Allen RM, Hauksson E. Determination of earthquake early warning parameters, tc and Pd, for southern California. GeophysJInt 2007;170:711–7.